JCI The Journal of Clinical Investigation

Subchondral bone osteoclasts induce sensory innervation and osteoarthritis pain

Shouan Zhu, … , Xinzhong Dong, Xu Cao

J Clin Invest. 2018. https://doi.org/10.1172/JCI121561.

Research In-Press Preview Bone biology Neuroscience

Graphical abstract

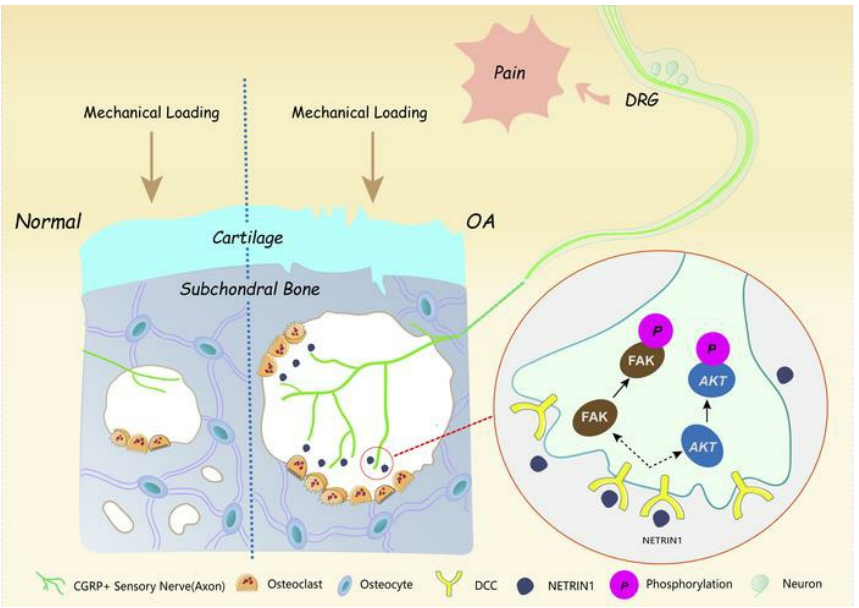

Subchondral bone osteoclasts induce sensory innervation and osteoarthritis pain

Shouan Zhu[1,2,#], Jianxi Zhu[1,3,#], Gehua Zhen[1], Yihe Hu[3], Senbo An[1,3], Yusheng Li[1,3], Qin Zheng[4], Zhiyong Chen[5], Ya Yang[5], Mei Wan[1], Richard Leroy Skolasky[1], Yong Cao[1], Tianding Wu[1], Bo Gao[1], Mi Yang[1], Manman Gao[1], Julia Kuliwaba[6], Shuangfei Ni[1], Lei Wang[1], Chuanlong Wu[1], David Findlay[6], Holger K. Eltzschig[7], Hong Wei Ouyang[2,8], Janet Crane[1], Feng-Quan Zhou[1], Yun Guan[5], Xinzhong Dong[4,9], and Xu Cao[1*]

[1]Department of Orthopaedic Surgery, The Johns Hopkins University School of Medicine, Baltimore, MD 21205, USA

[2]Dr. Li Dak Sum and Yip Yio Chin Center for Stem Cells and Regenerative Medicine, School of Medicine, Zhejiang University, Hangzhou, 310000, China

[3]Department of Orthopaedic Surgery, Xiangya Hospital, Central South University, Changsha, 410008, China

[4]Department of Neuroscience, Neurosurgery, and Dermatology, Center of Sensory Biology, The Johns Hopkins University School of Medicine, Howard Hughes Medical Institute, Baltimore, MD 21205, USA

[5]Department of Anesthesiology and Critical Care Medicine, The Johns Hopkins University School of Medicine, Baltimore, MD 21205, USA

[6]Department of Orthopaedics and Trauma, Royal Adelaide Hospital, the University of Adelaide, Adelaide, South Australia 5005, Australia

[7]Department of Anesthesiology, The University of Texas Health Science Center at Houston, McGovern Medical School, Houston, TX 77030, USA

[8]ZJU-UoE Joint institute, School of Medicine, Zhejiang University, Hangzhou, 310000, China

[#]These authors contributed equally to this work.

* Corresponding Author:
Xu Cao, Ph.D.
Email: xcao11@jhmi.edu
Mailing Address: 601 North Caroline Street/Suite 5214 Baltimore, MD 21287-0881
Phone: 410-502-6440

Acknowledgements

The authors thank Jenni Weems and Rachel Box in the editorial office at the Department of Orthopaedic Surgery, The Johns Hopkins University, for editing the manuscript. Funding: This work was supported by the NIH/NIAMS grants AR071432 and AR063943 (to X.C.) and NS070814 (to Y.G.). This work was facilitated by the Pain Research Core funded by the Blaustein Fund and the Neurosurgery Pain Research Institute at the Johns Hopkins University.

Declaration of interest statement

The authors have declared that no conflict of interest exists.

Abstract

Joint pain is the defining symptom of osteoarthritis (OA) but its origin and mechanisms remain unclear. Here, we investigated an unprecedented role of osteoclast-initiated subchondral bone remodeling in sensory innervation for OA pain. We show that osteoclasts secrete NETRIN1 to induce sensory nerve axonal growth in subchondral bone. Reduction of osteoclast formation by knockout of receptor activator of nuclear factor kappa-B ligand (*Rankl*) in osteocytes inhibited the growth of sensory nerves into subchondral bone, DRG neuron hyperexcitability, and behavioral measures of pain hypersensitivity in OA mice. Moreover, we demonstrated a possible role for NETRIN1 secreted by osteoclasts during aberrant subchondral bone remodeling in inducing sensory innervation and OA pain through its receptor DCC (deleted in colorectal cancer). Importantly, knockout of *Netrin1* in tartrate-resistant acid phosphatase (TRAP) positive osteoclasts or knockdown of *Dcc* reduces OA pain behavior. In particular, inhibition of osteoclast activity by alendronate modifies aberrant subchondral bone remodeling and reduces innervation and pain behavior at the early stage of OA. These results suggest that intervention of the axonal guidance molecules (e.g. NETRIN1) derived from aberrant subchondral bone remodeling may have therapeutic potential for OA pain.

Introduction

OA is a common musculoskeletal disease in adults and is estimated to affect 78 million people by 2040(1), leading to disability and reduced quality of life. Joint pain is the defining symptom of OA, and yet there is little understanding of its etiology(2). Currently, OA pain is inadequately controlled by analgesics and nonsteroidal anti-inflammatory drugs, with unsustained pain relief and substantial adverse effects(3). More recent humanized nerve growth factor (NGF) mAb holds great potential to alleviate pain in patients with severe OA(4). However, side effects including association with rapid progression of OA and osteonecrosis in the clinical trial, and autonomic nervous system toxicity in preclinical model(5) were detected. The observation implicates that better understanding of OA pain pathomechanisms is essential to develop disease-modifying therapy for OA pain.

Evidence from both clinical and preclinical studies suggests that continuous nociceptive input from the OA joint drives sensitization of both central and peripheral nervous system(6, 7). Central sensitization in the spinal cord and dysregulation of the ascending and descending pathway from brain through the spinal cord, at least partially explains widespread pain sensitivity in OA patients(8, 9). Additionally, modulation of an integrated network among glial cells, neurons, and immune cells in the dorsal root ganglia (DRG) and central nervous system has been shown to correlate with arthritis pain(10, 11). On the other hand, locally in osteoarthritic joints, cytokines, chemokines, and inflammatory factors, including tumor necrosis factor (TNF)(12), interleukin (IL)1(13, 14), IL6(15, 16), IL17(17, 18), NGF(19-22), prostaglandin E2(23, 24) can lead to hypersensitivity with exaggerated pain (hyperalgesia) by noxious stimuli or innocuous stimuli are perceived as painful (allodynia). Peripheral sensitization has been evaluated by behavioral testing in ample preclinical models to indicate OA pain(25). As a base for peripheral sensitization,

multiple tissues including synovium(26), ligament(27), osteochondral junction(28, 29) and meniscus(30) in the joint are densely innervated by perivascular sensory and sympathetic nerves. Examination of innervation changes in either animal models of OA or human specimens has reached inconsistent conclusions probably because different disease stages were observed. Two studies in the collagenase-induced model reported either a transient(31) or a permanent(32) decrease in synovial innervation, while another study in the DMM and *Pkcδ* null model reported increased synovial innervation(26). Neural element showed by gold chloride staining was initially reported to decrease in osteoarthritic posterior cruciate ligament (PCL)(33), while another study used immunohistochemistry for CGRP showed constant nociceptive sensory innervation in OA PCL(27). In particular, perivascular sensory and sympathetic nerve fibers have been observed breaching the osteochondral junction in OA(28, 29).

Subchondral bone may also be an important source of pain in OA, specifically, subchondral bone marrow edema–like lesions visualized by magnetic resonance imaging (MRI) highly correlated with OA pain(34, 35). Zoledronic acid, a drug that inhibits osteoclast activity, was effective in reducing OA knee pain and bone marrow edema–like lesion size(36). Analysis of a comprehensive dataset from the National Institutes of Health Osteoarthritis Initiative showed that bisphosphonate users experienced significantly reduced knee pain at 2 and 3 years(37). Increased subchondral bone remodeling occurs during OA progression(38). We reported previously that aberrant subchondral bone remodeling initiates joint articular cartilage degeneration(39). Specifically, elevated osteoclast activity activates excessive TGFB1 to recruit mesenchymal stem cells in the marrow, where they undergo aberrant subchondral bone formation. Systemic or local administration of TGFB1 neutralizing antibody (1D11) attenuated OA progression by targeting subchondral bone pathological features(40). The subchondral bone changes at the early stage of OA further suggest a potential pathogenesis of OA pain.

In the mammalian neuro-system, wiring of neuronal axons into tissues is directed by specific cues in the extracellular environment, a process called axon guidance (also called axon pathfinding). Guidance cues come in 4 types: NETRINs, SLITs, EPHRINs, and SEMAPHORINs. These signals can be fixed in place or diffusible; they can attract or repel axons. The neurite outgrowth includes elongation and branching(41) and is required by both attractive and repulsive cues to control, respectively, axon outgrowth and disassembly of adhesive structures together with cytoskeletal dynamics(42, 43). Interestingly, researchers using a combination of genetic and biochemical methods have found that axon guidance molecules, such as SEMAPHORINs, NETRINs, and EPHRINs, are also involved in differentiation and communication between osteoclasts and osteoblasts(44-51) essential for bone formation and skeletal homeostasis. SEMA3A has also been shown to regulate bone remodeling indirectly by modulating sensory nerve innervation(45). Here, we investigated the role of osteoclast-initiated subchondral bone remodeling in sensory innervation for pain hypersensitivity during OA progression. We found that an increase in osteoclasts in early OA was strongly related to the appearance and persistence of sensory nerves in the subchondral bone, with evidence for a role for osteoclast-derived NETRIN1 to mediate OA pain

Results

Sensory nerve innervation in subchondral bone correlates with osteoclast activity during OA progression.

We first examined the potential role of osteoclasts in sensory innervation in subchondral bone, because we have shown an increase in osteoclasts at the early stage of OA and angiogenesis induced by preosteoclasts(39, 52). Mouse anterior cruciate ligaments (ACLs) were transected to create an ACL transection (ACLT) OA model. The ACLT OA joints were harvested at different

time points for immunohistologic analysis of subchondral bone. At 2 weeks after surgery, we observed decreased proteoglycan staining (red) and a rough surface in articular cartilage, suggesting cartilage matrix degeneration. At 4 weeks after surgery, there were small cartilage lesions across the tibial articular cartilage with big lesions deep to calcified cartilage at 8 weeks (Fig. 1A, top). Tartrate-resistant acid phosphatase (TRAP) positive osteoclasts were increased in subchondral bone as early as 1 week after ACLT surgery and were maintained at a high level for 2 weeks (Fig. 1A, second row; Fig. 1B). Osteoclastic bone resorption generated large bone marrow cavities at 8 weeks (Fig. 1A, second row). We then examined the neurons that innervate subchondral bone. Both posterior and anterior areas of tibial subchondral bone were imaged and analyzed (Suppl. Fig. 2, whole joint calcitonin gene-related peptide [CGRP] immunostaining). Immunostaining of CGRP, a potent vasodilator that causes pain sensitization, showed aberrant distribution of peptidergic nociceptive nerve fibers adjacent to the trabecular bone surface beginning 1 week after surgery. The numbers and density of nerve endings remained increased at 8 weeks after ACLT surgery (Fig. 1A, third row; Fig. 1C). Very few TRAP+ osteoclasts and CGRP+ sensory nerve endings in subchondral bone were observed in sham groups at corresponding time points (Suppl. Fig. 1A and D). Based on a newly proposed classification of sensory neurons(53), we also stained another 3 markers of nociceptive neurons NF200, P2X2, and PIEZO2. Interestingly, the density of P2X2 and PIEZO2 are also increased while NF200 remained constant in subchondral bone marrow of ACLT operated mice (Suppl. Fig. 3A and B). Staining for other subsets of neuronal fibers, PGP9.5, and B TUBULIN in subchondral bone marrow showed minimal alterations by ACLT surgery (Suppl. Fig. 3A and B). Together, these results suggest that the overall innervation of different subgroups of nociceptive neurons is increased in OA subchondral bone. Because it has been shown that cartilage degeneration and subchondral bone destruction seem to develop preferentially at the posterior part of the knee(54), we further

analyzed the distribution of CGRP+ nerves in the 2 different compartments of subchondral bone. Interestingly, no significant difference was observed between the posterior and anterior compartments (Suppl. Fig. 3C).

To evaluate whether sensory nerve innervation in subchondral bone is associated with OA pain, we analyzed DRG neuron activity in *Pirt-GCaMP3* mice. In *Pirt-GCaMP3* mice, the entire coding region of the phosphoinositide-interacting regulator of TRP (*Pirt*) gene(55) which is expressed predominantly in nociceptive neurons was replaced with the Ca^{2+} indicator (GCaMP3) in frame with *Pirt* promoter so that DRG neurons expressed the genetically encoded Ca^{2+} sensitive indicator(56). This mouse model allows for the detection of increased peripheral neuronal activity in primary sensory neurons in the DRG. We observed significantly increased numbers of activated DRG neurons in response to mechanical force generated by a rodent pincher analgesia meter on the knee at 1 week after ACLT surgery, which had increased to 70 ± 5 neurons at 4 weeks and remained steady at 8 weeks (Fig. 1A, bottom; Fig. 1D). In contrast, an average of 5–8 neurons were activated by the same mechanical force in sham-operated mice (Suppl. Fig. 1B and C). Similar neuronal hyperexcitability in a destabilized medial meniscus (DMM) OA mouse model was also recently reported by Miller and colleagues(57).

To validate the increased number of DRG neurons responding to knee pinch through CGRP+ sensory innervation in subchondral bone, we conducted a retrograde labeling experiment using Dil in rats (rats were used instead of mice because of the technical difficulty of injecting dye into subchondral bone in mice). Indeed, the number of CGRP+ neurons labeled with Dil in L4-5 DRGs in the ACLT group was significantly greater than that in the sham-surgery group (Fig. 1E and F). The number of IB4+ neurons labeled with Dil was not significantly different between the 2 groups (Suppl. Fig. 3D and E). The total number of neurons labeled with Dil in the sham group

was 25 ± 5 (~5.2% were CGRP+). The total number of neurons labeled with Dil in the ACLT group was 31 ± 3 (~78.3% were CGRP+) (Fig. 1E and F).

To define the specific type of neurons that responded to knee pinch, we assessed the size distribution of the neurons activated by knee pinch during the time course of OA development. Before ACLT, a few neurons with area > 600 μm^2 were activated by ~20-g knee pinch, consistent with the size of non-nociceptive neurons. The number of small- to medium-sized neurons (area < 600 μm^2) increased continuously in response to knee pinch after surgery and became the majority of activated neurons at 8 weeks, consistent with the size of C and Aδ fiber neurons, which function primarily as nociceptors (Fig. 2A).

To examine whether the increased number of DRG neurons responding to knee pinch were the neuronal population responsible for OA pain, we tested whether they are also capsaicin sensitive. We performed both mechanical force–evoked, as well as capsaicin-evoked *in vivo* DRG imaging experiments on the same L4 DGR of the same OA mice. With knee pinch, 54 neurons were activated, 76% of which were also activated by a direct drop of capsaicin (1 μM) onto the DRG (Fig. 2B and C). Because capsaicin can activate a subset of primary afferent neurons associated with both pain and thermoreception, some large neurons with more brightness were activated only by capsaicin (Fig. 2B, white arrow).

Together, these findings suggest that an increase in osteoclast mediated bone resorption induces sensory innervation in the subchondral bone and hyperexcitability of DRG neurons. The high correlation between bone remodeling and innervation of nociceptive neurons in subchondral suggests that nociceptive neurons could potentially mediate OA pain and be targeted locally.

Sprouting of sensory nerves in subchondral bone and OA pain decreased in *Dmp1-Rankl$^{f/f}$* mice.

We next tested whether sensory innervation is initiated by osteoclasts and associated with OA pain. Dentin matrix acidic phosphoprotein 1 (*Dmp1*)-Cre mice were crossbred with receptor activator of nuclear factor kappa-B ligand (*Rankl*) floxed mice to knock out *Rankl* in DMP1+ osteocytes. DMP1+ osteocytes are the primary source of *Rankl* for osteoclast differentiation(58, 59). Deficiency of *Rankl* in osteocytes leads to a decrease in osteoclast number and a severe osteopetrotic phenotype(58, 59). TRAP+ osteoclasts were decreased in the subchondral bone surface in *Dmp1-Rank* $^{f/f}$-ACLT mice relative to *Rankl*$^{f/f}$-ACLT controls (Fig. 3A, first row; Fig. 3C). Importantly, the density of CGRP+ neurofilaments was markedly decreased in *Dmp1-Rankl*$^{f/f}$-ACLT mice (Fig. 3A. second row; Fig. 3B), suggesting that osteoclast activity was associated with CGRP+ sensory innervation in the subchondral bone. Moreover, the articular cartilage was protected in *Dmp1-Rankl*$^{f/f}$-ACLT mice, as indicated by proteoglycan staining (Fig. 3A, third row) and significantly lower Osteoarthritis Research Society International (OARSI) scores(51) than those of *Rankl*$^{f/f}$-ACLT controls (Fig. 3E). The tibial subchondral bone volume in the *Rankl*$^{f/f}$-ACLT mice was 20% higher than that of sham-surgery controls at 2 months after surgery by micro-computed tomography (μCT) analysis. Subchondral bone tissue volume increased slightly (not significant) in *Dmp1-Rankl*$^{f/f}$-ACLT mice (Fig. 3A, fourth row; Fig.3 D). The thickness of the subchondral bone plate was decreased in the *Rankl*$^{f/f}$-ACLT mice but remained the same in *Dmp1-Rankl*$^{f/f}$-ACLT mice at 2 months after surgery compared with the sham-surgery controls (Suppl. Fig. 4A). The trabecular pattern factor was increased in *Dmp1-Rankl*$^{f/f}$-ACLT mice, but not as much as that in *Rankl*$^{f/f}$-ACLT mice (Suppl. Fig. 4B). Immunostaining showed that the numbers of OSTERIX+ osteoblast progenitors and pSMAD2/3+ cells, which are indicators of increased bone remodeling(39, 60), also increased significantly in *Rankl*$^{f/f}$-ACLT controls but not in *Dmp1-Rankl*$^{f/f}$-ACLT mice, indicating minimal subchondral bone remodeling in the knockout mice (Suppl. Fig. 4C–E). Microfil contrast-enhanced

angiography also demonstrated abrogation of the increase in subchondral blood vessels in *Dmp1-Rankl*$^{f/f}$ mice relative to *Rankl*$^{f/f}$ mice after ACLT (Suppl. Fig. 4F–H). These results suggest that uncoupled bone remodeling was arrested in *Dmp1-Rankl*$^{f/f}$-ACLT mice and led to decreased sprouting of sensory nerves.

To examine whether sensory nerves in subchondral bone mediate OA pain, we next cross-bred *Dmp1-Rankl*$^{f/f}$ with *Pirt-GCaMP3* mice. Compared with that in *Rankl*$^{f/f}$;*Pirt-GCaMP3*-ACLT mice, the number of DRG neurons activated by knee pinch was significantly decreased in *Dmp1-Rankl*$^{f/f}$;*Pirt-GCaMP3*-ACLT mice (Fig. 3F and G). The intensity of responding neurons was then analyzed. The maximum magnitude and duration of response between wild-type (WT) and conditional knockout (KO) mice remained the same in response to mechanical force (Fig. 3H). Secondary allodynia assessed by von Frey(61) showed that there was a significant decrease in the paw withdrawal thresholds (PWTs) induced by ACLT in *Rankl*$^{f/f}$ control mice by 1 week that persisted through 16 weeks (Fig. 3I). *Dmp1-Rankl*$^{f/f}$ mice had a significant decrease in PWT 1 week after ACLT, but PWT was soon upregulated and was similar to that of sham-surgery controls by 2 weeks (Fig. 3I). Furthermore, ink blot analysis revealed a significant disparity between the percentage of right hind paw ipsilateral intensity (Fig. 2J and K) and contact area (Fig. 2J and L) of the 2 limbs at 1 month after ACLT surgery in *Rankl*$^{f/f}$ controls relative to sham-surgery controls, which was not observed in *Dmp1-Rankl*$^{f/f}$-ACLT mice. No significant changes were observed between *Rankl*$^{f/f}$ and *Dmp1-Rankl*$^{f/f}$ mice in ipsilateral stride length or hind paw base of support (BOS) (Suppl. Fig. 4I and J). Together, these results indicate that sensory innervation induced by subchondral bone osteoclasts may mediate OA pain.

NETRIN1 secreted by osteoclasts and axonal growth

To examine the molecular mechanism by which osteoclasts regulate axonal growth, we cultured macrophages/monocytes to differentiate into osteoclasts, as evidenced by TRAP+ staining and the number of nuclei (Suppl. Fig. 5). The conditioned media of macrophages/monocytes and osteoclasts were collected to screen potential factors from osteoclasts that could promote axonal growth. Primary DRG neurons were collected from adult mice and cultured on the cellular side of a microfluidic culture platform, an *in vitro* method used widely in studies of axonal injury and regeneration by probing axons independently from cell bodies(62). The wells on the axonal side were filled with different conditioned media. Osteoclast-conditioned media induced growth of axons across the microchannels into the axonal side. However, macrophage/monocyte-conditioned media had little effect on axonal growth (Fig. 4A). This finding suggests that one or more diffusible factors were secreted in the osteoclast-conditioned media and promoted axonal growth. To identify the potential secreted factor(s), we added functional blocking antibodies against SLIT3, EPHRINB2, SEMA3A, and NETRIN1 to the conditioned media. The antibody against NETRIN1 inhibited the axonal growth induced by the osteoclast-conditioned media, whereas other antibodies were ineffective (Fig. 4A and B). Consistent with this finding, the addition of mouse recombinant NETRIN1 peptide promoted axonal outgrowth (Fig. 3C and D).

To examine the signaling mechanisms of NETRIN1 induced axon growth, we tested whether NETRIN1 activates focal adhesion kinase (FAK) and PI3K/Akt pathways(63). Notably, NETRIN1 induced phosphorylation of FAK and AKT at 30 min, peaking at 90 min (Fig. 4E). Interestingly, NETRIN1 expression was noted primarily in mature osteoclast-extracted protein as shown in Western blot analysis (Fig. 4F) and further confirmed by enzyme-linked immunosorbent assay (ELISA) in the osteoclast-conditioned media (Fig. 4G). Furthermore, immunostaining demonstrated that NETRIN1 co-localized with TRAP staining and was significantly higher on the bone surface 2 weeks after ACLT surgery, decreasing to baseline level at 4 and 8 weeks after

ACLT surgery (Fig. 4H and I). We then measured the concentrations of NETRIN1 in subchondral bone marrow in *Dmp1-Rankl*$^{f/f}$ and *Rankl*$^{f/f}$ mice. ACLT-operated *Rankl*$^{f/f}$ control mice had increased concentrations of NETRIN1 in subchondral bone marrow relative to sham-surgery *Rankl*$^{f/f}$ mice (Fig. 4J). The concentration of NETRIN1 was higher in *Dmp1-Rankl*$^{f/f}$ mice relative to *Rankl*$^{f/f}$ controls but did not increase significantly after ACLT surgery relative to sham-operated controls (Fig. 4J). In addition, we examined NETRIN1 expression in the subchondral bone of human knee joints with OA. There were more TRAP+ osteoclasts expressing NETRIN1 in OA subchondral bone than there were in healthy controls (Fig. 5A–B, Table 1). Taken together, these findings demonstrate that osteoclasts-induced subchondral bone remodeling mediates OA pain, with a possible role for NETRIN1 in promoting sensory innervation progression.

Knockout of *Netrin1* in TRAP+ osteoclasts reduced sensory innervation in OA subchondral bone and OA pain.

We then examined the functions of NETRIN1 secreted by osteoclasts in subchondral sensory innervation *in vivo*. We crossbred *Netrin1* floxed mice (*Ntn*$^{f/f}$ mice) with *Trap-Cre* mice to generate *Trap-Ntn*$^{f/f}$ mice with the deletion of *Netrin1* in the TRAP+ cell lineage. The concentration of NETRIN1 decreased significantly in the subchondral bone of *Trap-Ntn*$^{f/f}$ mice relative to their WT littermates operated with ACLT according to ELISA (Fig. 6A). Additionally, *in vitro* Western blot assay and immunostaining showed significantly decreased NETRIN1 in the subchondral bone of *Trap-Ntn*$^{f/f}$ mice (Suppl. Fig. 6A and B). Safranin orange and fast green staining showed similar cartilage degeneration in WT and *Trap-Ntn*$^{f/f}$ mice after ACLT (Fig. 6B), as also reflected in OARSI scores (Fig. 6C). The tibial subchondral bone also showed similar changes in *Trap-Ntn*$^{f/f}$ mice and WT littermates (Fig. 6D and Suppl. Fig. 6C and D) after ACLT surgery. Moreover, the subchondral bone remodeling rate (as indicated by number of OSTERIX+ osteoblast progenitors

and pSMAD2/3+ cells) increased similarly in *Ntn*$^{f/f}$ and *Trap-Ntn*$^{f/f}$ mice after ACLT (Suppl. Fig. 6G–I), suggesting that *Netrin1* does not mediate OA progression. Importantly, although the number of TRAP+ osteoclasts increased after ACLT in the *Trap-Ntn*$^{f/f}$ mice (Fig. 6E, top; Fig. 6F), the density of CGRP+ sensory nerves was similar to that of sham-surgery controls (Fig. 6E, bottom; Fig. 6G). These findings suggest that NETRIN1 secreted by osteoclasts plays an important role for sensory nerve innervation into subchondral bone.

We also measured DRG neuron activation in response to mechanical force. *Trap-Ntn*$^{f/f}$ mice were crossed with *Pirt-GCaMP3* mice to yield *Trap-Ntn*$^{f/-}$;*Pirt-GCaMP3* mice with calcium indicator expression in DRG neurons. Because mouse *Pirt* (chromosome 11, NC_000077.6, 66911910..66929877) and *Netrin1* (chromosome 11, NC_000077.6, 68209364..68386826, complement) are in close proximity, per the law of linkage and crossing-over, no homozygous *Ntn*$^{f/f}$;*Pirt-GCaMP3* mice were obtained. ELISA analysis confirmed that 1 allele deletion of *Netrin1* in osteoclasts was sufficient to significantly decrease NETRIN1 concentration in OA subchondral bone (Suppl. Fig. 7C). Consistently, although some CGRP+ sensory fibers could be seen in the subchondral bone of the heterozygous *Netrin1* KO mice after ACLT, the density of CGRP+ nerve endings (Suppl. Fig. 7A and B) and the number of activated DRG neurons (Fig. 6H and I) in *Trap-Ntn*$^{f/-}$;*Pirt-GCaMP3* mice were significantly less than those in *Ntn*$^{f/f}$;*Pirt-GCaMP3* mice after ACLT. The intensity of neuronal responses was then analyzed. The maximum magnitude and duration between *Ntn*$^{f/f}$;*Pirt-GCaMP3* and *Trap-Ntn*$^{f/-}$;*Pirt-GCaMP3* remained the same in response to mechanical force (Fig. 4J).

To test whether sensory innervation in subchondral bone mediates OA pain, we measured PWTs in *Trap-Ntn*$^{f/f}$ mice. A significantly decreased PWT was sustained in *Ntn*$^{f/f}$ mice at 1–16 weeks after ACLT surgery (Fig. 6K). However, in *Trap-Ntn*$^{f/f}$ mice, the decreased PWT did not persist, becoming upregulated after the acute phase of 1 week (Fig. 6K). A similar though less

effective upregulation of PWT was also seen in *Netrin1* heterozygous *Trap-Ntn*$^{f/-}$ mice (Suppl. Fig. 7D). Ink blot analysis revealed a significant disparity in the percentage of right hind paw ipsilateral intensity (Fig. 6L and M) and contact area (Fig. 6L and N) in WT mice after ACLT surgery that was abrogated in ACLT *Trap-Ntn*$^{f/f}$ mice. No differences in right hind paw ipsilateral stride length nor percentage of hind paw BOS were observed between *Ntn*$^{f/f}$ and *Trap-Ntn*$^{f/f}$ ACTL and sham-surgery groups (Suppl. Fig. 6E and F). Thus, NETRIN1 secreted from osteoclast lineage cells stimulates sensory innervation into OA subchondral bone to mediate chronic OA pain but has no effect on OA progression.

NETRIN1 promoted sensory innervation through its DCC receptor.

To identify the receptor for NETRIN1 that promotes neuronal growth, we first used *in vitro* microfluidic assays with DRG neurons treated with scramble, anti-*Dcc*, or anti-*Unc5* small interfering RNAs (siRNAs). Knockdown of the expression of *Dcc*, but not *Unc5*, blocked the axonal protrusion induced by osteoclast-conditioned media (Fig. 7A), suggesting that NETRIN1 exerts its attractive functions through DCC. We next tested the requirement of DCC for sensory nerve fiber innervation into subchondral bone *in vivo*. We developed Ambion *in vivo* siRNA by tail vein injection. Knockdown of *Dcc* by injection of siRNA into the WT mouse tail vein did not halt the progression of OA, as indicated by similar degeneration of cartilage in the knee joint and OARSI score (Fig. 7B, top; Fig. 7C). However, the numbers of sensory fibers positive for DCC (Fig. 7B, middle; Fig. 7C) and CGRP (Fig. 7B, bottom; Fig. 7C) were decreased significantly in the ACLT group treated with *siDcc* compared with those treated with scramble siRNA. We further tested whether inhibition of sensory innervation by Ambion *in vivo siDcc* could ameliorate OA pain behavior. PWTs in *siDcc* treated ACLT mice were significantly higher than in scramble siRNA-treated ACLT mice 4 weeks after surgery and persisted through 8 weeks (Fig. 7D). Gait

parameters were then measured using the CatWalk gait analysis system. In scramble siRNA–inoculated ACLT mice, left hind/right hind (LH/RH) paw pressure (light intensity), LH/RH print area ratio, and swing speed were significantly decreased, which were all abrogated in *siDcc* treated ACLT mice (Fig. 7E). Together, these findings suggest that inhibition of DCC expression in subchondral bone reduced OA pain after ACLT surgery.

Inhibition of osteoclasts by alendronate (ALN) ameliorated OA pain and disease progression. Bisphosphonates are an anti-resorptive class of drugs that inhibit osteoclast resorptive activity and induce osteoclast apoptosis(64). The bisphosphonate ALN has been shown to be a potentially useful therapeutic agent for slowing the development of OA through chondroprotective effects and inhibition of subchondral bone remodeling in various surgical animal models(65-67). Compared with ACLT-induced OA, DMM-induced OA results in imbalanced joint biomechanics that lead to relatively slow disease progression and are usually considered more clinically relevant(68). Moreover, it has been demonstrated that standard analgesics can reverse pain in DMM mice, making this model ideal to test the effect of analgesics on OA pain development (10). Thus, for our intervention studies, the DMM model was used to test the effect of alendronate on OA pain relief. Time course analysis of NETRIN1 levels in subchondral bone revealed that the density of NETRIN1 staining was significantly higher 2 weeks after DMM compared with the sham group and peaked at 4 weeks (Suppl. Fig. 8A and B). This seems to be a delayed response compared with that in subchondral bone of ACLT mice, which is in consistent with slower disease progression in the DMM model. Similar to the results in ACLT mice, immunostaining of CGRP in DMM mice showed an increasing distribution of peptidergic nociceptive nerve fibers adjacent to the trabecular bone surface beginning 1 week after surgery (Suppl. Fig. 8A and C). The numbers and density of nerve endings remained increased at 8 weeks after DMM surgery. 8 weeks after DMM surgery,

vehicle-treated mice had loss of safranin orange staining, fibrous/defective surface cartilage, and significantly elevated OARSI scores (Fig. 8A, top; Fig 8B, top). Similar to the ACLT OA model, DMM mice also had increased TRAP+ osteoclasts (Fig. 8A, middle; Fig. 8B, middle) and CGRP+ sensory nerves (Fig. 8A, bottom; Fig. 8B, bottom) in the subchondral bone. ALN treatment attenuated OA progression, the number of TRAP+ osteoclasts, and the number of CGRP+ sensory nerves (Fig. 8A and B, middle and bottom). ALN treatment also reduced the NETRIN1 staining in subchondral bone (Fig. 8C). Moreover, the decreased PWT after DMM was attenuated in the ALN-treated DMM mice at 4 weeks, which persisted at 8 weeks relative to vehicle-treated mice (Fig. 8D). Using CatWalk gait analysis, we found that DMM surgery resulted in similar decreases of LH/RH print area, duty cycle, and swing speed and increased swing phase. These were prevented by ALN treatment (Fig. 8E), suggesting that inhibition of osteoclast activity by ALN ameliorates OA pain.

Discussion

Current OA pain management strategies have limited therapeutic effects, and progressive pathological joint changes are observed frequently with these treatments. The 2012 American College of Rheumatology guidelines recommend analgesics and non-steroidal anti-inflammatory drugs as the first-line pharmacologic therapies for OA of the hand, hip, and knee(69). However, these drugs provide insufficient and unsustained pain relief with considerable adverse effects. Our previous study revealed that excessive activation of TGFB1 during subchondral bone remodeling recruits mesenchymal stem cells for aberrant bone formation and angiogenesis, which is a key step in the pathogenesis of OA(39, 70). In the current study, we report that osteoclast-initiated subchondral bone remodeling mediates OA pain, with a possible role for osteoclast-secreted NETRIN1. For the first time, we revealed that nociceptors are generated during aberrant

subchondral bone remodeling in the early phase of OA. Our findings suggest that inhibition of aberrant subchondral bone formation can reduce sensory innervation and attenuate articular cartilage degeneration.

Articular cartilage and subchondral bone are not only a mechanical unit but also a biological functional unit(71). The structural alterations of subchondral bone in OA are believed to enhance its capacity for cross-talk with articular cartilage. In this study, we observed significant protection of articular cartilage from degeneration in *Dmp1-Rankl*$^{f/f}$ mice, suggesting that active subchondral bone remodeling in response to abnormal mechanical loading is critical for OA progression. Specifically, the decreased number of osteoclasts in *Dmp1-Rankl*$^{f/f}$ mice led to significantly reduced hyperexcitability of DRG neurons to mechanical stimulation applied to OA joints. Consistent with previous reports(26, 28), an increased number of CGRP+ sensory nerves was seen in the synovium of both *Dmp1-Rankl*$^{f/f}$ (Suppl. Fig. 9A and B) and *Trap-Ntn*$^{f/f}$ (Suppl. Fig. 9C and D) mice after OA surgery in our study. However, the density of CGRP+ neurofilaments in subchondral bone was decreased in *Dmp1-Rankl*$^{f/f}$ and *Trap-Ntn*$^{f/f}$ mice. These results further indicate that osteoclasts in aberrant subchondral bone remodeling could be an important origin of OA pain. The various methods used to measure pain in this study are complementary. We examined mechanical hypersensitivity to *von Frey* filament stimulation applied to hindpaw in OA animals. Mechanical hypersensitivity of hindpaw may represent the secondary hyperalgesia developed after OA. Activation and sensitization of nociceptive neurons (peripheral sensitization) may contribute to the hyperalgesia at the knee joint (e.g., pinch-evoked pain hypersensitivity at the joint and movement-induced behavioral changes). Indeed, our *in vivo* GCaMP3 image experiments also have indicated a hypersensitivity of DRG neurons to stimulation at the knee. It is important to note that continued nociceptive input may also induce central sensitization (e.g., increase of spinal dorsal horn neurons excitability) that would amplify the afferent input from the

diseased joint and also lead to secondary hyperalgesia in other somatic body regions (e.g., hindpaw). Indeed, central sensitization has been evidenced by many clinical and animal studies to contribute to the lack of direct correlation between nociceptor activation and the pain. Primary hyperalgesia in OA knees has recently been investigated by measuring withdraw threshold in responding to direct knee pinching or press using a pressure application measurement (PAM) device in mice DMM model(72). Future study integrating this method of pain measurement would further complement our current study.

The increased remodeling rate in subchondral bone is initiated by osteoclasts and is a known pathological feature of OA, particularly during the early stage of disease(38). Osteoclastic lineage cells are the principal, if not exclusive, bone-resorbing cells essential for bone remodeling and skeletal development. Osteochondral junctions have long been implicated as early sites of new blood vessel growth, which is accompanied by extensions of sympathetic and sensory nerves in OA(28, 29). Blood vessel and nerve growth are linked by common pathways activated during the release of proangiogenic factors(73). Our study has identified a possible role for NETRIN1 secreted by osteoclasts during aberrant subchondral bone remodeling in inducing sensory innervation and OA pain. In addition to its role in axon guidance, NETRIN1 has been suggested to be a potent vascular mitogen(74-76). NETRIN1 was found to promote angiogenesis by controlling endothelial cell migration(75), tubal formation(77), and apoptosis blockade(78). Our previous study revealed that preosteoclasts secrete platelet-derived growth factor-BB during bone remodeling to induce angiogenesis coupled with osteogenesis during bone formation(52). Thus, osteoclast lineage cells may promote both nerve and vessel growth in OA subchondral bone, leading to disease progression and pain.

We acknowledge that other mechanisms may exist for osteoclast activation–induced OA pain. For example, osteoclasts are believed to play multiple roles in cancer-associated bone pain (CABP)(79). Specifically, osteoclasts secret proton from bone resorption sites via the α3 vacuolar-proton-ATPase signaling pathway, acidifying the extracellular bone microenvironment. Acidosis is algogenic for nociceptive sensory neurons that innervate into bone. Acidic environments upregulate and activate pH-sensitive acid-sensing nociceptors, the transient receptor potential channel-vanilloid subfamily member 1 (TRPV1), and acid-sensing ion channels (ASIC3) to evoke CABP. In our study, we also observed activation of osteoclasts in the subchondral bone during early stages of OA. We think the activation of osteoclasts is bifunctional. On one hand, osteoclast-secreted NETRIN1 facilitates peptidergic neurite growth. On the other hand, the osteoclastic resorption may also create an acidic environment in subchondral bone that peripherally sensitizes the nociceptive neurons. Moreover, NETRIN1 was also found to activate TRPV1 in dorsal horn neurons(80). Thus, it is possible that NETRIN1 itself could also peripherally sensitize nociceptive neurons.

Neuroanatomical and molecular characterization of nociceptors demonstrates the heterogeneity of C-fibers(81). The peptidergic subpopulation of nociceptors release neuropeptides, such as substance P and CGRP, and express tropomyosin receptor kinase A. The nonpeptidergic subpopulation of nociceptors expresses the c-Ret receptor. A large percentage of the c-Ret–positive population also binds the isolectin IB4 and expresses G protein–coupled receptors of the Mrg family(82). Our retrograde labeling data showed a significant increase in the number of CGRP+ nociceptors that newly innervated into OA subchondral bone marrow. Immunofluorescence studies showed that the density of NF200, PGP9.5, and B TUBULIN in subchondral bone marrow was not altered by ACLT. We observed that the density of CGRP+ and other nociceptive nerve endings (e.g. P2X3 and PIEZO2) increased, while PGP9.5+ nerve density

remained unchanged in OA subchondral bone. Protein gene product (PGP), also known as ubiquitin carboxy-terminal hydrolase 1 (UCHL1), is a pan neuronal marker that labels most peptidergic and non-peptidergic, nociceptive, and non-nociceptive neurons. Our observation suggests that innervation of other non-CGRP-expressing neuronal populations might decrease, leaving the total density of PGP9.5+ nerves unchanged. Indeed, a recent study(83) using a UCHL1-eGFP reporter line found that ~64% of bright DRG eGFP+ neurons expressed CGRP, while the other ~36% neurons did not, indicating that CGRP+ subpopulations exist in PGP9.5-expressing neurons. We acknowledge that determining how dynamic changes in subpopulations of neurons innervate into subchondral bone in response to ACLT will require different genetic methods in our future work. Our findings agree with the observation in recent studies that the percentage of CGRP+ neurons innervating subchondral bone augmented significantly after OA induction(84). Yet, the way in which these nociceptive neurons innervate subchondral bone marrow during OA progression remains to be investigated.

Mice deficient in *Netrin1* exhibited less OA pain and minimal alterations in gait, even though they developed rapid proteoglycan loss in articular cartilage, as did WT mice. *Netrin1* conditional KO mice showed similar increases in subchondral bone volume and trabecular pattern factor after OA as those seen in WT mice. Accordingly, inhibition of innervation of CGRP+ sensory fibers in the subchondral bone reduced OA pain but did not affect subchondral bone remodeling or articular cartilage degeneration, suggesting a dissociation between pain perception and joint destruction. An extreme example of this dissociation is “Charcot’s joint,” a process marked by bony destruction, bone resorption, and eventual deformity caused by loss of sensation(85). One well-accepted explanation of this pathogenesis is neurotrauma. Loss of peripheral sensation and proprioception leads to repetitive microtrauma to the joint(86). Mediero and colleagues reported a similar increase of NETRIN1 expression during osteoclast

differentiation, with an autocrine and paracrine manner binding to UNC5B to promote osteoclast differentiation(48). Interestingly, our *Netrin1* conditional KO mice have a similar subchondral bone remodeling rate as that of WT mice. This could be attributable to different microenvironments in subchondral bone versus diaphyseal bone, especially in pathological conditions such as OA, in which a combination of cytokines, chemokines, and inflammatory factors affect osteoclast/osteoblast differentiation in joints locally. NETRIN1 has been shown to bind/interact with various receptors, including DCC, UNC5 homologues, and adenosine A2B receptor. In agreement with other studies, our results showed that NETRIN1 promoted DRG neuron axonal outgrowth and subchondral bone sensory innervation through the DCC receptor. Adenosine A2B receptor has been shown to bind directly to DCC and function as a NETRIN1 co-receptor(87). In addition, recent studies have reported that NETRIN1 signaling through the adenosine A2B receptor inhibits diabetic nephropathy(88) and hypoxia-induced inflammatory cell infiltration into mucosal organs(89). Inhibition of adenosine receptors by caffeine has been used frequently as an adjuvant analgesic in combination with nonsteroidal anti-inflammatory drugs or opioids(90, 91). Thus, it would be of interest in future studies to further examine the expression of the adenosine A2B receptor in the peripheral nerve system and its involvement in NETRIN1 induced axonal outgrowth in osteoarthritis subchondral bone.

The inhibition of excessive TGFB1 activity or osteoclast bone resorption, such as by using bisphosphonate, may interrupt aberrant subchondral bone remodeling and reduce innervation of CGRP+ sensory fibers in the subchondral bone to attenuate OA pain. Indeed, bisphosphonates have been tested in OA clinical trials(92-95) and achieved some beneficial effects on articular cartilage and marrow lesions, improved Western Ontario and McMaster Universities Osteoarthritis Index pain scores, and decreased prevalence of subchondral bone marrow lesions. However, the reported effects of bisphosphonates have been mixed(96). The lack of efficacy in some studies

may be explained by the heterogeneity of pathogenesis. Our previous study showed that uncoupled aberrant subchondral bone formation led to articular cartilage degeneration. Active subchondral bone resorption releases excessive active TGFB1, which recruits mesenchymal stem cells to the subchondral bone marrow for aberrant bone formation along with type H vessel formation during the early stage of OA(39, 70). During the middle and late stages of OA, uncoupled abnormal bone formation has largely finished, with limited osteoclast activity(39). Accordingly, the optimal time for bisphosphonate treatment would be during the early stage of OA because this is the period when sensory innervation is induced by osteoclasts.

Given the increasing incidence of OA and the insufficient control of OA pain by current available medication, better understanding of the mechanisms of OA pain would potentially help develop more effective analgesics. Our study has identified that aberrant subchondral bone remodeling initiated by osteoclasts induces sensory innervation, with a possible of NETRIN1. Inhibition of osteoclast activity by alendronate modifies aberrant subchondral bone remodeling and reduces innervation and pain behavior at the onset of OA. Our study suggests that intervention of the axonal guidance molecules (e.g. NETRIN1) derived from aberrant subchondral bone remodeling may have therapeutic potential for OA pain.

Methods

Mice

We purchased C57BL/6J (WT) male mice from Charles River Laboratories. We anesthetized the mice at 2 months of age with ketamine and xylazine and then transected the ACL surgically to induce mechanical instability–associated osteoarthritis of the right knee. Sham operations were performed on other groups of mice. In the sham groups, the knee capsule and infrapatellar fat pad were incised but no ACL transection was performed. For the time-course experiments, mice were

euthanized at 0, 1, 2, 4, or 8 weeks after surgery (n = 8 per group). DMM surgery was performed in the left knees of mice. Briefly, the surgery started with a 3-mm longitudinal incision over the distal patella to the proximal tibial plateau. The anterior medial meniscotibial ligament was identified and resected with the blade directed proximolaterally to destabilize the medial meniscus. Sham surgery followed the same procedure to expose the anterior medial meniscotibial ligament, but the ligament was left intact. Mice were not administered analgesia after surgery. ALN was injected intraperitoneally 3 times per week at a dose of 1mg/kg for 8 weeks after DMM surgery.

CatWalk analysis

Gait parameters of freely moving mice were measured using the CatWalk gait analysis system (Noldus Information Technology) as described previously(97). Briefly, the CatWalk instrument consists of an enclosed walkway with a glass plate floor, a fluorescent lamp that emits light inside the glass plate, a high-speed color video camera, and recording and analysis software to assess the gait of rodents. Each mouse was placed individually in the CatWalk walkway and allowed to walk freely and traverse from one side to the other of the walkway. Mice were trained as described previously(98). The recordings were made when the room was completely dark, except for the light from the computer screen. Where the mouse paws made contact with the glass plate, light was reflected down and the illuminated contact areas recorded with a high-speed color video camera that was positioned under the glass plate and connected to a computer running the CatWalk software, v7.1. The software automatically labeled all areas containing pixels above the set threshold (7 pixels). These areas were identified and assigned to the respective paws. The recording generated a wide range of parameters, the following 7 of which were analyzed: Paw pressure, Paw print area, Stance phase, Swing phase, Duty cycle, Stride length, Swing speed (Please see detailed information about the 7 parameters in supplementary methods).

Statistical analysis

Data are presented as means ± standard deviations. Error bars represent standard deviations. We used unpaired, 2-tailed Student t-tests for comparisons between 2 groups, and 1-way analysis of variance with Bonferroni *post hoc* test for multiple comparisons. For all experiments, $P < 0.05$ was considered to be significant and is indicated by *; $P < 0.01$ is indicated by **. All inclusion/exclusion criteria were pre-established, and no samples or animals were excluded from the analysis. No statistical method was used to predetermine the sample size. The experiments were randomized. The investigators were blinded to allocation during experiments and outcome assessment. Specifically, each animal was assigned an identification number using the animal's litter number in combination with the ear tag number. The investigators who conducted experiments (e.g., ACLT/DMM surgery, siRNA injections, ALN injections) were blinded to animal genotypes. Outcome assessments (e.g., OARSI grading) were conducted by 2 independent graders who were not involved directly in the experiments, and outcomes were recorded in the order of animal identification number.

Study approval

Human OA cartilage was obtained from patients undergoing total knee replacement surgery at the Department of Orthopaedic Surgery in Xiangya Hospital (Central South University, Changsha, China). Normal (control) cartilage was obtained postmortem from human subjects with no history of OA. The patients' consent, as well as approval of the local ethics committees, were obtained before harvesting human tissue samples. We maintained all animals in the animal facility of The Johns Hopkins University School of Medicine (Baltimore, MD, USA). The experimental protocol was reviewed and approved by the Institutional Animal Care and Use Committee of The Johns Hopkins University.

583

Author Contributions

S.Z. and J.Z. conceived the ideas for experimental designs, conducted most of the experiments, and prepared the manuscript. G.Z., M.W., and R.S. provided some ideas and helped with behavior analysis. S.A., Y.L., and B.G. helped with histology sections and animal surgery. Q.Z., Z.C., and Y.Y. helped with *in vivo* DRG imaging. Y.C., T.W., M.Y., M.G., S.N., L.W., and C.W. helped with immunostaining and human sample histology. J.K. and D.F. provided some of the human OA samples. E.H. provided *Netrin1* floxed mice. Y.G. helped with behavioral tests and helped write the manuscript. J.C. helped with manuscript revisions. Y.H., H.W.O., X.D., and F-Q.Z. provided suggestions for the project. X.C. developed the concept, supervised the project, conceived the experiments, and wrote most of the manuscript.

Acknowledgments

This study was supported by National Institutes of Health grants AR063943 (to X.C.) and NS070814 (to Y.G.). This work was facilitated by the Pain Research Core funded by the Blaustein Fund and the Neurosurgery Pain Research Institute at The Johns Hopkins University, as well as a training award (to S.Z.) from China Scholarship Council. The authors thank Rachel Box in the editorial office at the department of Orthopaedic Surgery, the Johns Hopkins University, for editing the manuscript.

References

1. Hootman JM, Helmick CG, Barbour KE, Theis KA, and Boring MA. Updated Projected Prevalence of Self-Reported Doctor-Diagnosed Arthritis and Arthritis-Attributable Activity Limitation Among US Adults, 2015-2040. *Arthritis Rheumatol.* 2016;68(7):1582-7.
2. Hunter DJ, McDougall JJ, and Keefe FJ. The symptoms of osteoarthritis and the genesis of pain. *Med Clin North Am.* 2009;93(1):83-100, xi.
3. O'Neil CK, Hanlon JT, and Marcum ZA. Adverse effects of analgesics commonly used by older adults with osteoarthritis: focus on non-opioid and opioid analgesics. *Am J Geriatr Pharmacother.* 2012;10(6):331-42.
4. Lane NE, Schnitzer TJ, Birbara CA, Mokhtarani M, Shelton DL, Smith MD, et al. Tanezumab for the treatment of pain from osteoarthritis of the knee. *N Engl J Med.* 2010;363(16):1521-31.
5. Mullard A. Drug developers reboot anti-NGF pain programmes. *Nat Rev Drug Discov.* 2015;14(5):297-8.
6. Schaible HG, Richter F, Ebersberger A, Boettger MK, Vanegas H, Natura G, et al. Joint pain. *Exp Brain Res.* 2009;196(1):153-62.
7. Suokas AK, Walsh DA, McWilliams DF, Condon L, Moreton B, Wylde V, et al. Quantitative sensory testing in painful osteoarthritis: a systematic review and meta-analysis. *Osteoarthritis Cartilage.* 2012;20(10):1075-85.
8. Hassan H, and Walsh DA. Central pain processing in osteoarthritis: implications for treatment. *Pain Manag.* 2014;4(1):45-56.
9. Lluch E, Torres R, Nijs J, and Van Oosterwijck J. Evidence for central sensitization in patients with osteoarthritis pain: a systematic literature review. *Eur J Pain.* 2014;18(10):1367-75.
10. Miller RE, Tran PB, Das R, Ghoreishi-Haack N, Ren D, Miller RJ, et al. CCR2 chemokine receptor signaling mediates pain in experimental osteoarthritis. *Proc Natl Acad Sci U S A.* 2012;109(50):20602-7.
11. Segond von Banchet G, Boettger MK, Fischer N, Gajda M, Brauer R, and Schaible HG. Experimental arthritis causes tumor necrosis factor-alpha-dependent infiltration of macrophages into rat dorsal root ganglia which correlates with pain-related behavior. *Pain.* 2009;145(1-2):151-9.
12. Jin X, and Gereau RWt. Acute p38-mediated modulation of tetrodotoxin-resistant sodium channels in mouse sensory neurons by tumor necrosis factor-alpha. *J Neurosci.* 2006;26(1):246-55.

13. Ebbinghaus M, Uhlig B, Richter F, von Banchet GS, Gajda M, Brauer R, et al. The role of interleukin-1beta in arthritic pain: main involvement in thermal, but not mechanical, hyperalgesia in rat antigen-induced arthritis. *Arthritis Rheum.* 2012;64(12):3897-907.
14. von Banchet GS, Fischer N, Uhlig B, Hensellek S, Eitner A, and Schaible HG. Molecular effects of interleukin-1beta on dorsal root ganglion neurons: prevention of ligand-induced internalization of the bradykinin 2 receptor and downregulation of G protein-coupled receptor kinase 2. *Mol Cell Neurosci.* 2011;46(1):262-71.
15. Obreja O, Biasio W, Andratsch M, Lips KS, Rathee PK, Ludwig A, et al. Fast modulation of heat-activated ionic current by proinflammatory interleukin 6 in rat sensory neurons. *Brain.* 2005;128(Pt 7):1634-41.
16. von Banchet GS, Kiehl M, and Schaible HG. Acute and long-term effects of IL-6 on cultured dorsal root ganglion neurones from adult rat. *J Neurochem.* 2005;94(1):238-48.
17. Richter F, Natura G, Ebbinghaus M, von Banchet GS, Hensellek S, Konig C, et al. Interleukin-17 sensitizes joint nociceptors to mechanical stimuli and contributes to arthritic pain through neuronal interleukin-17 receptors in rodents. *Arthritis Rheum.* 2012;64(12):4125-34.
18. Segond von Banchet G, Boettger MK, Konig C, Iwakura Y, Brauer R, and Schaible HG. Neuronal IL-17 receptor upregulates TRPV4 but not TRPV1 receptors in DRG neurons and mediates mechanical but not thermal hyperalgesia. *Mol Cell Neurosci.* 2013;52:152-60.
19. Ashraf S, Mapp PI, Burston J, Bennett AJ, Chapman V, and Walsh DA. Augmented pain behavioural responses to intra-articular injection of nerve growth factor in two animal models of osteoarthritis. *Ann Rheum Dis.* 2014;73(9):1710-8.
20. Nwosu LN, Mapp PI, Chapman V, and Walsh DA. Blocking the tropomyosin receptor kinase A (TrkA) receptor inhibits pain behaviour in two rat models of osteoarthritis. *Ann Rheum Dis.* 2016;75(6):1246-54.
21. Sagar DR, Nwosu L, Walsh DA, and Chapman V. Dissecting the contribution of knee joint NGF to spinal nociceptive sensitization in a model of OA pain in the rat. *Osteoarthritis Cartilage.* 2015;23(6):906-13.
22. Woolf CJ, Safieh-Garabedian B, Ma QP, Crilly P, and Winter J. Nerve growth factor contributes to the generation of inflammatory sensory hypersensitivity. *Neuroscience.* 1994;62(2):327-31.
23. Miller RJ, Jung H, Bhangoo SK, and White FA. Cytokine and chemokine regulation of sensory neuron function. *Handb Exp Pharmacol.* 2009(194):417-49.
24. Vane JR. The mode of action of aspirin-like drugs. *Agents Actions.* 1978;8(4):430-1.

25. Syx D, Tran PB, Miller RE, and Malfait AM. Peripheral Mechanisms Contributing to Osteoarthritis Pain. *Curr Rheumatol Rep.* 2018;20(2):9.
26. Kc R, Li X, Kroin JS, Liu Z, Chen D, Xiao G, et al. PKCdelta null mutations in a mouse model of osteoarthritis alter osteoarthritic pain independently of joint pathology by augmenting NGF/TrkA-induced axonal outgrowth. *Ann Rheum Dis.* 2016;75(12):2133-41.
27. Ikeuchi M, Wang Q, Izumi M, and Tani T. Nociceptive sensory innervation of the posterior cruciate ligament in osteoarthritic knees. *Arch Orthop Trauma Surg.* 2012;132(6):891-5.
28. Mapp PI, and Walsh DA. Mechanisms and targets of angiogenesis and nerve growth in osteoarthritis. *Nat Rev Rheumatol.* 2012;8(7):390-8.
29. Suri S, Gill SE, Massena de Camin S, Wilson D, McWilliams DF, and Walsh DA. Neurovascular invasion at the osteochondral junction and in osteophytes in osteoarthritis. *Ann Rheum Dis.* 2007;66(11):1423-8.
30. Malfait AM, and Schnitzer TJ. Towards a mechanism-based approach to pain management in osteoarthritis. *Nat Rev Rheumatol.* 2013;9(11):654-64.
31. Murakami K, Nakagawa H, Nishimura K, and Matsuo S. Changes in peptidergic fiber density in the synovium of mice with collagenase-induced acute arthritis. *Can J Physiol Pharmacol.* 2015;93(6):435-41.
32. Buma P, Verschuren C, Versleyen D, Van der Kraan P, and Oestreicher AB. Calcitonin gene-related peptide, substance P and GAP-43/B-50 immunoreactivity in the normal and arthrotic knee joint of the mouse. *Histochemistry.* 1992;98(5):327-39.
33. Franchi A, Zaccherotti G, and Aglietti P. Neural system of the human posterior cruciate ligament in osteoarthritis. *J Arthroplasty.* 1995;10(5):679-82.
34. Kwoh CK. Clinical relevance of bone marrow lesions in OA. *Nat Rev Rheumatol.* 2013;9(1):7-8.
35. Yusuf E, Kortekaas MC, Watt I, Huizinga TW, and Kloppenburg M. Do knee abnormalities visualised on MRI explain knee pain in knee osteoarthritis? A systematic review. *Ann Rheum Dis.* 2011;70(1):60-7.
36. Laslett LL, Dore DA, Quinn SJ, Boon P, Ryan E, Winzenberg TM, et al. Zoledronic acid reduces knee pain and bone marrow lesions over 1 year: a randomised controlled trial. *Ann Rheum Dis.* 2012;71(8):1322-8.
37. Laslett LL, Kingsbury SR, Hensor EM, Bowes MA, and Conaghan PG. Effect of bisphosphonate use in patients with symptomatic and radiographic knee osteoarthritis: data from the Osteoarthritis Initiative. *Ann Rheum Dis.* 2014;73(5):824-30.

38. Zhen G, and Cao X. Targeting TGFbeta signaling in subchondral bone and articular cartilage homeostasis. *Trends Pharmacol Sci.* 2014;35(5):227-36.
39. Zhen G, Wen C, Jia X, Li Y, Crane JL, Mears SC, et al. Inhibition of TGF-beta signaling in mesenchymal stem cells of subchondral bone attenuates osteoarthritis. *Nat Med.* 2013;19(6):704-12.
40. Xie L, Tintani F, Wang X, Li F, Zhen G, Qiu T, et al. Systemic neutralization of TGF-beta attenuates osteoarthritis. *Ann N Y Acad Sci.* 2016;1376(1):53-64.
41. Raper J, and Mason C. Cellular strategies of axonal pathfinding. *Cold Spring Harb Perspect Biol.* 2010;2(9):a001933.
42. Chacon MR, and Fazzari P. FAK: dynamic integration of guidance signals at the growth cone. *Cell Adh Migr.* 2011;5(1):52-5.
43. Moore SW, Zhang X, Lynch CD, and Sheetz MP. Netrin-1 attracts axons through FAK-dependent mechanotransduction. *J Neurosci.* 2012;32(34):11574-85.
44. Delorme G, Saltel F, Bonnelye E, Jurdic P, and Machuca-Gayet I. Expression and function of semaphorin 7A in bone cells. *Biol Cell.* 2005;97(7):589-97.
45. Fukuda T, Takeda S, Xu R, Ochi H, Sunamura S, Sato T, et al. Sema3A regulates bone-mass accrual through sensory innervations. *Nature.* 2013;497(7450):490-3.
46. Irie N, Takada Y, Watanabe Y, Matsuzaki Y, Naruse C, Asano M, et al. Bidirectional signaling through ephrinA2-EphA2 enhances osteoclastogenesis and suppresses osteoblastogenesis. *J Biol Chem.* 2009;284(21):14637-44.
47. Maruyama K, Kawasaki T, Hamaguchi M, Hashimoto M, Furu M, Ito H, et al. Bone-protective Functions of Netrin 1 Protein. *J Biol Chem.* 2016;291(46):23854-68.
48. Mediero A, Ramkhelawon B, Perez-Aso M, Moore KJ, and Cronstein BN. Netrin-1 is a critical autocrine/paracrine factor for osteoclast differentiation. *J Bone Miner Res.* 2015;30(5):837-54.
49. Sutton AL, Zhang X, Dowd DR, Kharode YP, Komm BS, and Macdonald PN. Semaphorin 3B is a 1,25-Dihydroxyvitamin D3-induced gene in osteoblasts that promotes osteoclastogenesis and induces osteopenia in mice. *Mol Endocrinol.* 2008;22(6):1370-81.
50. Takegahara N, Takamatsu H, Toyofuku T, Tsujimura T, Okuno T, Yukawa K, et al. Plexin-A1 and its interaction with DAP12 in immune responses and bone homeostasis. *Nat Cell Biol.* 2006;8(6):615-22.
51. Zhao C, Irie N, Takada Y, Shimoda K, Miyamoto T, Nishiwaki T, et al. Bidirectional ephrinB2-EphB4 signaling controls bone homeostasis. *Cell Metab.* 2006;4(2):111-21.
52. Xie H, Cui Z, Wang L, Xia Z, Hu Y, Xian L, et al. PDGF-BB secreted by preosteoclasts induces angiogenesis during coupling with osteogenesis. *Nat Med.* 2014;20(11):1270-8.

53. Usoskin D, Furlan A, Islam S, Abdo H, Lonnerberg P, Lou D, et al. Unbiased classification of sensory neuron types by large-scale single-cell RNA sequencing. *Nat Neurosci.* 2015;18(1):145-53.
54. Glasson SS, Blanchet TJ, and Morris EA. The surgical destabilization of the medial meniscus (DMM) model of osteoarthritis in the 129/SvEv mouse. *Osteoarthritis Cartilage.* 2007;15(9):1061-9.
55. Kim AY, Tang Z, Liu Q, Patel KN, Maag D, Geng Y, et al. Pirt, a phosphoinositide-binding protein, functions as a regulatory subunit of TRPV1. *Cell.* 2008;133(3):475-85.
56. Kim YS, Chu Y, Han L, Li M, Li Z, LaVinka PC, et al. Central terminal sensitization of TRPV1 by descending serotonergic facilitation modulates chronic pain. *Neuron.* 2014;81(4):873-87.
57. Miller RE, Kim YS, Tran PB, Ishihara S, Dong X, Miller RJ, et al. Visualization of Peripheral Neuron Sensitization in a Surgical Mouse Model of Osteoarthritis by In Vivo Calcium Imaging. *Arthritis Rheumatol.* 2018;70(1):88-97.
58. Nakashima T, Hayashi M, Fukunaga T, Kurata K, Oh-Hora M, Feng JQ, et al. Evidence for osteocyte regulation of bone homeostasis through RANKL expression. *Nat Med.* 2011;17(10):1231-4.
59. Xiong J, Onal M, Jilka RL, Weinstein RS, Manolagas SC, and O'Brien CA. Matrix-embedded cells control osteoclast formation. *Nat Med.* 2011;17(10):1235-41.
60. Tang Y, Wu X, Lei W, Pang L, Wan C, Shi Z, et al. TGF-beta1-induced migration of bone mesenchymal stem cells couples bone resorption with formation. *Nat Med.* 2009;15(7):757-65.
61. Chaplan SR, Bach FW, Pogrel JW, Chung JM, and Yaksh TL. Quantitative assessment of tactile allodynia in the rat paw. *J Neurosci Methods.* 1994;53(1):55-63.
62. Taylor AM, Blurton-Jones M, Rhee SW, Cribbs DH, Cotman CW, and Jeon NL. A microfluidic culture platform for CNS axonal injury, regeneration and transport. *Nat Methods.* 2005;2(8):599-605.
63. Bashaw GJ, and Klein R. Signaling from axon guidance receptors. *Cold Spring Harb Perspect Biol.* 2010;2(5):a001941.
64. Chen JS, and Sambrook PN. Antiresorptive therapies for osteoporosis: a clinical overview. *Nat Rev Endocrinol.* 2011;8(2):81-91.
65. Ding M, Danielsen CC, and Hvid I. The effects of bone remodeling inhibition by alendronate on three-dimensional microarchitecture of subchondral bone tissues in guinea pig primary osteoarthrosis. *Calcif Tissue Int.* 2008;82(1):77-86.
66. Hayami T, Pickarski M, Wesolowski GA, McLane J, Bone A, Destefano J, et al. The role of subchondral bone remodeling in osteoarthritis: reduction of cartilage degeneration and

prevention of osteophyte formation by alendronate in the rat anterior cruciate ligament transection model. *Arthritis Rheum.* 2004;50(4):1193-206.
67. Jones MD, Tran CW, Li G, Maksymowych WP, Zernicke RF, and Doschak MR. In vivo microfocal computed tomography and micro-magnetic resonance imaging evaluation of antiresorptive and antiinflammatory drugs as preventive treatments of osteoarthritis in the rat. *Arthritis Rheum.* 2010;62(9):2726-35.
68. Fang H, and Beier F. Mouse models of osteoarthritis: modelling risk factors and assessing outcomes. *Nat Rev Rheumatol.* 2014;10(7):413-21.
69. Hochberg MC, Altman RD, April KT, Benkhalti M, Guyatt G, McGowan J, et al. American College of Rheumatology 2012 recommendations for the use of nonpharmacologic and pharmacologic therapies in osteoarthritis of the hand, hip, and knee. *Arthritis Care Res (Hoboken).* 2012;64(4):465-74.
70. Cui Z, Crane J, Xie H, Jin X, Zhen G, Li C, et al. Halofuginone attenuates osteoarthritis by inhibition of TGF-beta activity and H-type vessel formation in subchondral bone. *Ann Rheum Dis.* 2016;75(9):1714-21.
71. Sharma AR, Jagga S, Lee SS, and Nam JS. Interplay between cartilage and subchondral bone contributing to pathogenesis of osteoarthritis. *Int J Mol Sci.* 2013;14(10):19805-30.
72. Miller RE, Ishihara S, Bhattacharyya B, Delaney A, Menichella DM, Miller RJ, et al. Chemogenetic Inhibition of Pain Neurons in a Mouse Model of Osteoarthritis. *Arthritis Rheumatol.* 2017;69(7):1429-39.
73. Vogel G. Developmental biology. The unexpected brains behind blood vessel growth. *Science.* 2005;307(5710):665-7.
74. Layne K, Ferro A, and Passacquale G. Netrin-1 as a novel therapeutic target in cardiovascular disease: to activate or inhibit? *Cardiovasc Res.* 2015;107(4):410-9.
75. Park KW, Crouse D, Lee M, Karnik SK, Sorensen LK, Murphy KJ, et al. The axonal attractant Netrin-1 is an angiogenic factor. *Proc Natl Acad Sci U S A.* 2004;101(46):16210-5.
76. Wilson BD, Ii M, Park KW, Suli A, Sorensen LK, Larrieu-Lahargue F, et al. Netrins promote developmental and therapeutic angiogenesis. *Science.* 2006;313(5787):640-4.
77. Tu T, Zhang C, Yan H, Luo Y, Kong R, Wen P, et al. CD146 acts as a novel receptor for netrin-1 in promoting angiogenesis and vascular development. *Cell Res.* 2015;25(3):275-87.
78. Mehlen P, and Furne C. Netrin-1: when a neuronal guidance cue turns out to be a regulator of tumorigenesis. *Cell Mol Life Sci.* 2005;62(22):2599-616.
79. Yoneda T, Hiasa M, Nagata Y, Okui T, and White FA. Acidic microenvironment and bone pain in cancer-colonized bone. *Bonekey Rep.* 2015;4:690.

80. Wu CH, Yuan XC, Gao F, Li HP, Cao J, Liu YS, et al. Netrin-1 Contributes to Myelinated Afferent Fiber Sprouting and Neuropathic Pain. *Mol Neurobiol.* 2016;53(8):5640-51.
81. Snider WD, and McMahon SB. Tackling pain at the source: new ideas about nociceptors. *Neuron.* 1998;20(4):629-32.
82. Dong X, Han S, Zylka MJ, Simon MI, and Anderson DJ. A diverse family of GPCRs expressed in specific subsets of nociceptive sensory neurons. *Cell.* 2001;106(5):619-32.
83. Genc B, Lagrimas AK, Kuru P, Hess R, Tu MW, Menichella DM, et al. Visualization of Sensory Neurons and Their Projections in an Upper Motor Neuron Reporter Line. *PLoS One.* 2015;10(7):e0132815.
84. Aso K, Izumi M, Sugimura N, Okanoue Y, Ushida T, and Ikeuchi M. Nociceptive phenotype alterations of dorsal root ganglia neurons innervating the subchondral bone in osteoarthritic rat knee joints. *Osteoarthritis Cartilage.* 2016;24(9):1596-603.
85. Varma AK. Charcot neuroarthropathy of the foot and ankle: a review. *J Foot Ankle Surg.* 2013;52(6):740-9.
86. Larson SA, and Burns PR. The pathogenesis of Charcot neuroarthropathy: current concepts. *Diabet Foot Ankle.* 2012;3.
87. Corset V, Nguyen-Ba-Charvet KT, Forcet C, Moyse E, Chedotal A, and Mehlen P. Netrin-1-mediated axon outgrowth and cAMP production requires interaction with adenosine A2b receptor. *Nature.* 2000;407(6805):747-50.
88. Tak E, Ridyard D, Badulak A, Giebler A, Shabeka U, Werner T, et al. Protective role for netrin-1 during diabetic nephropathy. *J Mol Med (Berl).* 2013;91(9):1071-80.
89. Rosenberger P, Schwab JM, Mirakaj V, Masekowsky E, Mager A, Morote-Garcia JC, et al. Hypoxia-inducible factor-dependent induction of netrin-1 dampens inflammation caused by hypoxia. *Nat Immunol.* 2009;10(2):195-202.
90. Abo-Salem OM, Hayallah AM, Bilkei-Gorzo A, Filipek B, Zimmer A, and Muller CE. Antinociceptive effects of novel A2B adenosine receptor antagonists. *J Pharmacol Exp Ther.* 2004;308(1):358-66.
91. Sawynok J, and Yaksh TL. Caffeine as an analgesic adjuvant: a review of pharmacology and mechanisms of action. *Pharmacol Rev.* 1993;45(1):43-85.
92. Bingham CO, 3rd, Buckland-Wright JC, Garnero P, Cohen SB, Dougados M, Adami S, et al. Risedronate decreases biochemical markers of cartilage degradation but does not decrease symptoms or slow radiographic progression in patients with medial compartment osteoarthritis of the knee: results of the two-year multinational knee osteoarthritis structural arthritis study. *Arthritis Rheum.* 2006;54(11):3494-507.

93. Buckland-Wright JC, Messent EA, Bingham CO, 3rd, Ward RJ, and Tonkin C. A 2 yr longitudinal radiographic study examining the effect of a bisphosphonate (risedronate) upon subchondral bone loss in osteoarthritic knee patients. *Rheumatology (Oxford).* 2007;46(2):257-64.
94. Raisz L, Smith JA, Trahiotis M, Fall P, Shoukri K, Digennaro J, et al. Short-term risedronate treatment in postmenopausal women: effects on biochemical markers of bone turnover. *Osteoporos Int.* 2000;11(7):615-20.
95. Spector TD, Conaghan PG, Buckland-Wright JC, Garnero P, Cline GA, Beary JF, et al. Effect of risedronate on joint structure and symptoms of knee osteoarthritis: results of the BRISK randomized, controlled trial [ISRCTN01928173]. *Arthritis Res Ther.* 2005;7(3):R625-33.
96. Castaneda S, Roman-Blas JA, Largo R, and Herrero-Beaumont G. Subchondral bone as a key target for osteoarthritis treatment. *Biochem Pharmacol.* 2012;83(3):315-23.
97. Solomon LA, Russell BA, Watson LA, Beier F, and Berube NG. Targeted loss of the ATR-X syndrome protein in the limb mesenchyme of mice causes brachydactyly. *Hum Mol Genet.* 2013;22(24):5015-25.
98. Hamers FP, Lankhorst AJ, van Laar TJ, Veldhuis WB, and Gispen WH. Automated quantitative gait analysis during overground locomotion in the rat: its application to spinal cord contusion and transection injuries. *J Neurotrauma.* 2001;18(2):187-201.

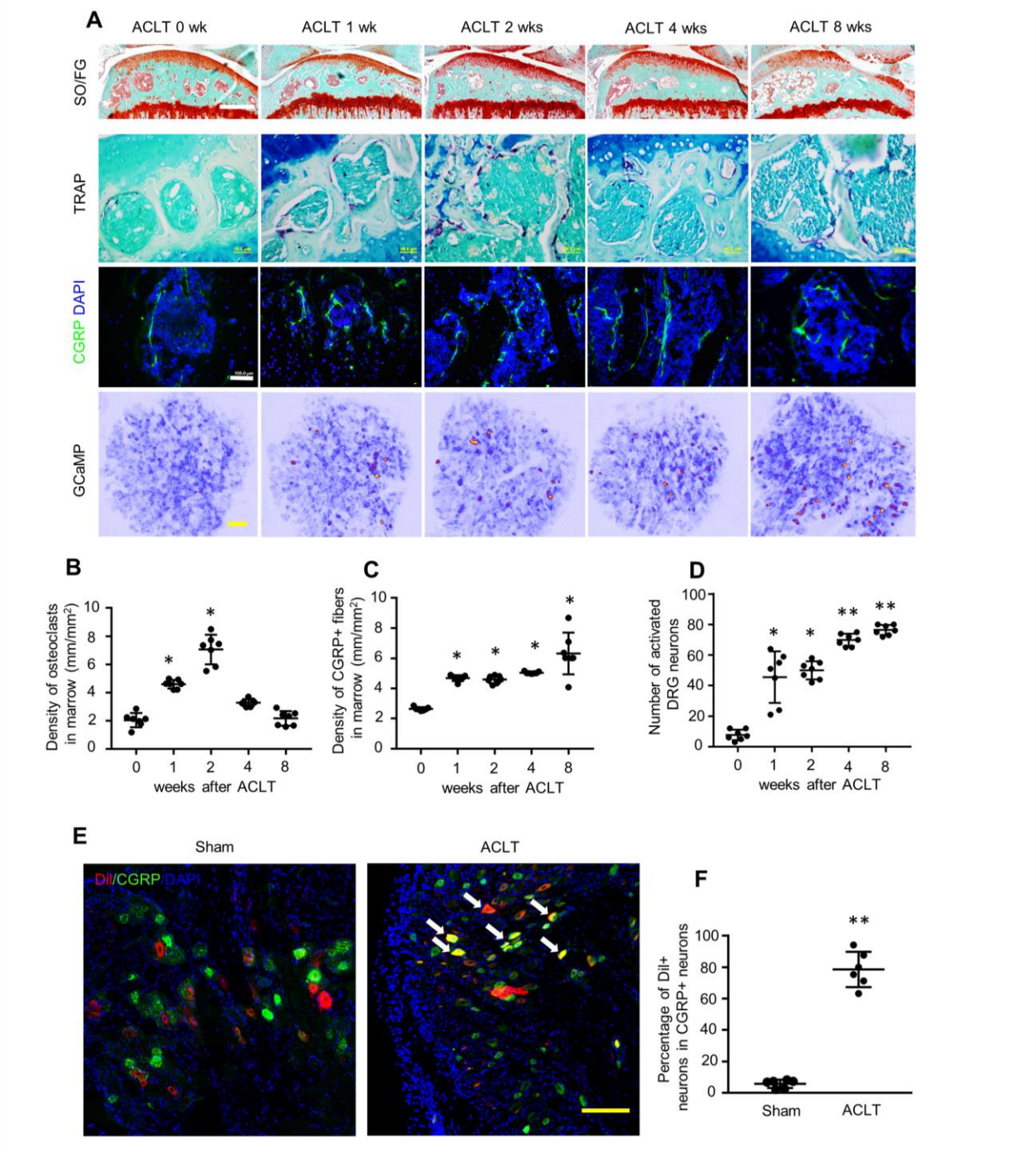

870

871 **Figure 1** CGRP+ sensory nerves in subchondral bone increased along with an increase in
872 osteoclast activity and DRG neuron hypersensitivity during OA progression. **(A)** Safranin orange
873 staining (top), TRAP staining (2nd row, magenta) and immunofluorescent analysis of CGRP+
874 sensory nerve fibers (3rd row, green) in mouse tibial subchondral bone after ACLT surgery at

different time points. Scale bars, 500 μm (top), 100 μm (2nd row), 50 μm (3rd row). Excitability (bottom) of L4 DRG in *Pirt-GCaMP3* mice at different time points after surgery. Scale bar, 100 μm. $n = 7$ per time point. (See full videos of neuronal hyperactivity in supplementary materials.) **(B, C)** Quantitative analysis of density of TRAP+ and CGRP+ sensory nerves in subchondral bone marrow. *$p < 0.05$ compared with the sham-operated group at the corresponding time points. $n = 7$ per time point. **(D)** Quantification of lit up DRG neurons. *$p < 0.05$, **$p < 0.01$ compared with the sham-operated group at the corresponding time points. $n = 7$ per group. **(E)** Representative photomicrographs of CGRP and Dil double-labeled neurons in L4 DRG. Scale bar, 50 μm. $n = 6$ per group. **(F)** Percentage of L4 DRG neurons retrogradely labeled Dil in all CGRP+ neurons 10 weeks after sham or ACLT surgery. ****$p < 0.01$ compared with the sham-operated group at the corresponding time points. Statistical significance was determined by multifactorial ANOVA, and all data are shown as means ± standard deviations.

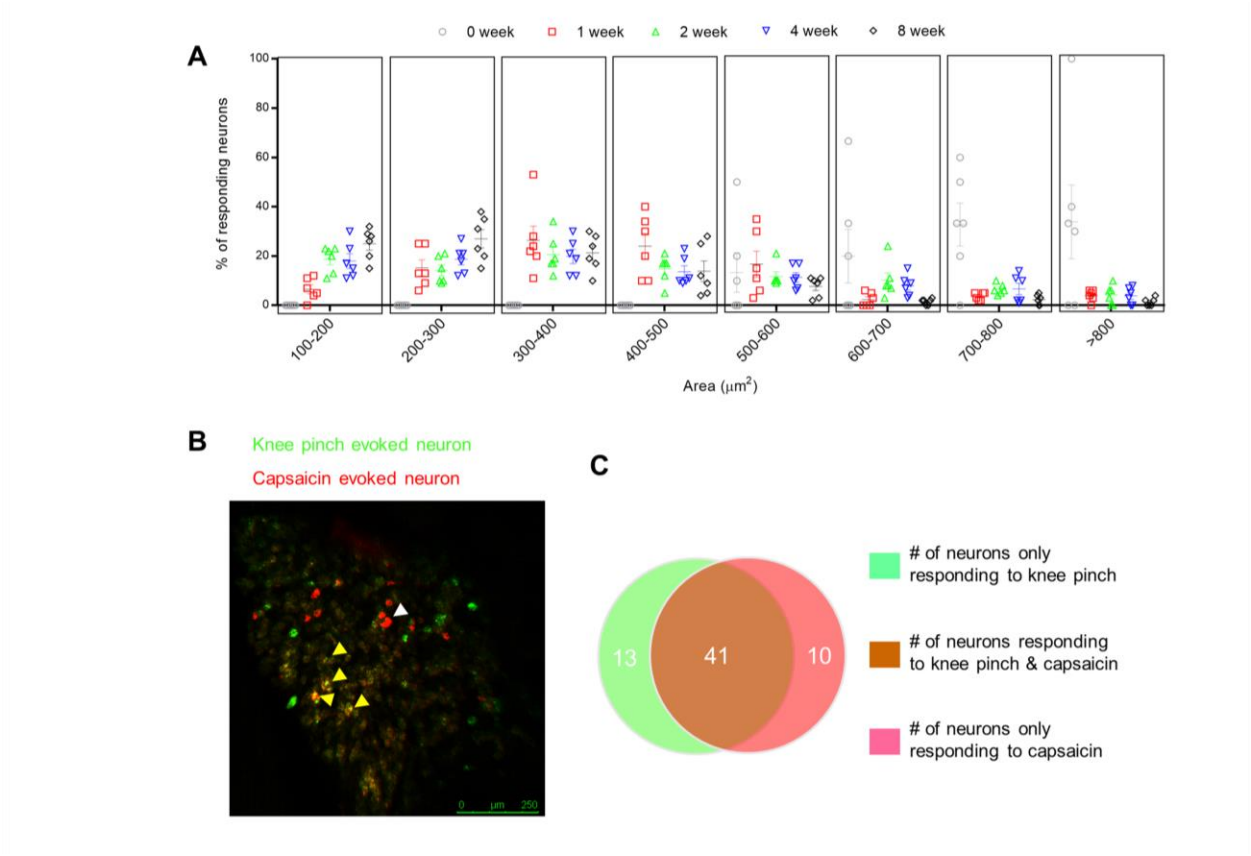

888

889 **Figure 2** In OA, most DRG neurons responding to knee pinch are nociceptive neurons. **(A)**
890 Relative frequency distributions of the areas of neurons responding to 20-g knee pinch in ACLT
891 mice at different time points. Mean ± standard deviation. **(B)** Excitability of L4 DRG in *Pirt-*
892 *GCaMP3* mice responding to knee pinch or direct drop of 1 μM of capsaicin. White arrows indicate
893 neurons responding only to capsaicin; yellow arrows indicate neurons responding to both knee
894 pinch and capsaicin. **(C)** Number of DRG neurons responding to knee pinch or capsaicin.

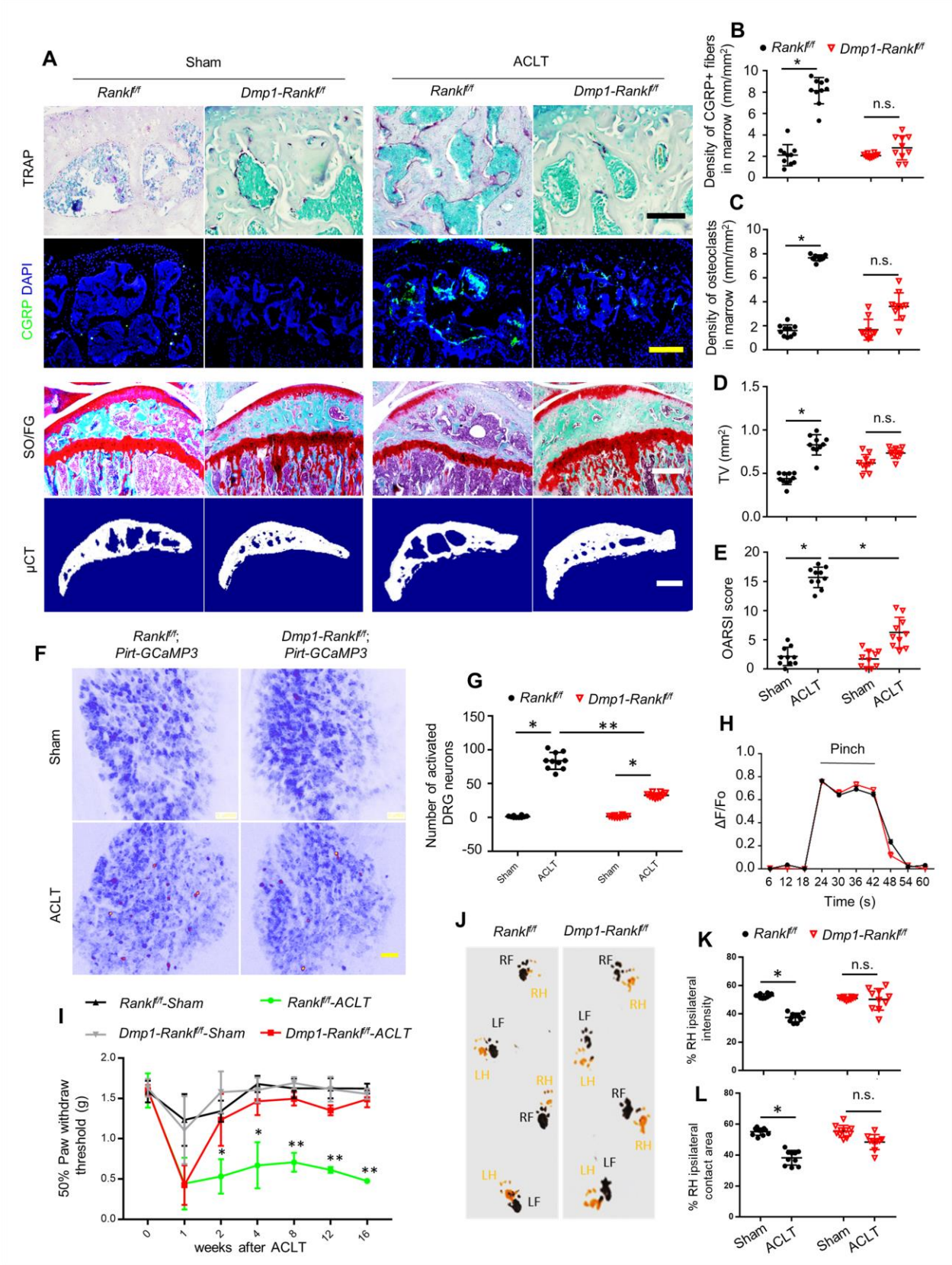
A
Sham
ACLT
Rankl f/f
Dmp1-Rankl f/f
TRAP
CGRP DAPI
SO/FG
µCT
B
Density of CGRP+ fibers in marrow (mm/mm²)
n.s.
C
Density of osteoclasts in marrow (mm/mm²)
D
TV (mm²)
E
OARSI score
Sham
ACLT
F
Rankl f/f; Pirt-GCaMP3
Dmp1-Rankl f/f; Pirt-GCaMP3
G
Number of activated DRG neurons
H
Pinch
ΔF/Fo
Time (s)
I
Rankl f/f-Sham
Rankl f/f-ACLT
Dmp1-Rankl f/f-Sham
Dmp1-Rankl f/f-ACLT
50% Paw withdraw threshold (g)
weeks after ACLT
J
RF
RH
LF
LH
K
% RH ipsilateral intensity
L
% RH ipsilateral contact area

Figure 3 Decreased sprouting of CGRP+ sensory nerves in the subchondral bone and amelioration of pain in *Dmp1-Rankl*$^{f/f}$ mice. **(A)** TRAP staining (1st row, magenta) and immunofluorescent analysis of CGRP+ sensory nerve fibers (2nd row, green) in mouse tibial subchondral bone after ACLT surgery. Scale bars, 100 μm. 3rd row, safranin orange and fast green staining of articular cartilage in sagittal sections of tibia medial compartment of *Rankl*$^{f/f}$ and *Dmp1-Rankl*$^{f/f}$ mice with or without ACLT surgery. Scale bar, 500 μm. 4th row, 3-dimensional μCT image of the tibia subchondral bone medial compartment (sagittal view) of *Rankl*$^{f/f}$ and *Dmp1-Rankl*$^{f/f}$ mice with or without ACLT surgery. Scale bar, 1 mm. $n = 9$ per group. **(B,C)** Quantitative analysis of the density of TRAP+ osteoclasts and CGRP+ nerve fibers in subchondral bone marrow. **(D,E)** Quantitative analysis of total tissue volume (TV) **(D)** and OARSI scores 8 weeks after surgery **(E)**. *$p < 0.05$, n.s = no significance. $n = 9$ per group. **(F)** *In vivo* calcium imaging in whole L4 DRG primary sensory neurons after mechanical press to knees of *Rankl*$^{f/f}$;*Pirt-GCaMP3* and *Dmp1-Rankl*$^{f/f}$;*Pirt-GCaMP3* mice. Scale bar, 50 μm. $n = 10$ per group. **(G)** Number of neurons activated by mechanical press. *$p < 0.05$, **$p < 0.01$. **(H)** Mean ± standard deviation of ΔF/Fo for neurons in a representative DRG responding to ~20-g paw pinch in *Rankl*$^{f/f}$ (black) and *Dmp1- Rankl*$^{f/f}$ (red) mice after ACLT. **(I)** Paw withdrawal threshold (PWT) was tested at the right hind paw of *Rankl*$^{f/f}$-sham, *Rankl*$^{f/f}$-ACLT, *Dmp1- Rankl*$^{f/f}$-sham, and *Dmp1- Rankl*$^{f/f}$-ACLT mice. *$p < 0.05$, **$p < 0.01$. **(J)** Representative images of ink blotting trial of *Rankl*$^{f/f}$ and *Dmp1-Rankl*$^{f/f}$ mice after ACLT surgery on right knees. RH = right hind (orange), LH = left hind (orange), RF = right front (black), LF = left front (black). **(K, L)** Quantitative analysis of percentage RH ipsilateral intensity (**K**) and percentage RH ipsilateral contact area (**L**) were measured and calculated using Image J software. *$p < 0.05$. $n = 10$ per group. Statistical significance was determined by multifactorial ANOVA, and all data are shown as means ± standard deviations.

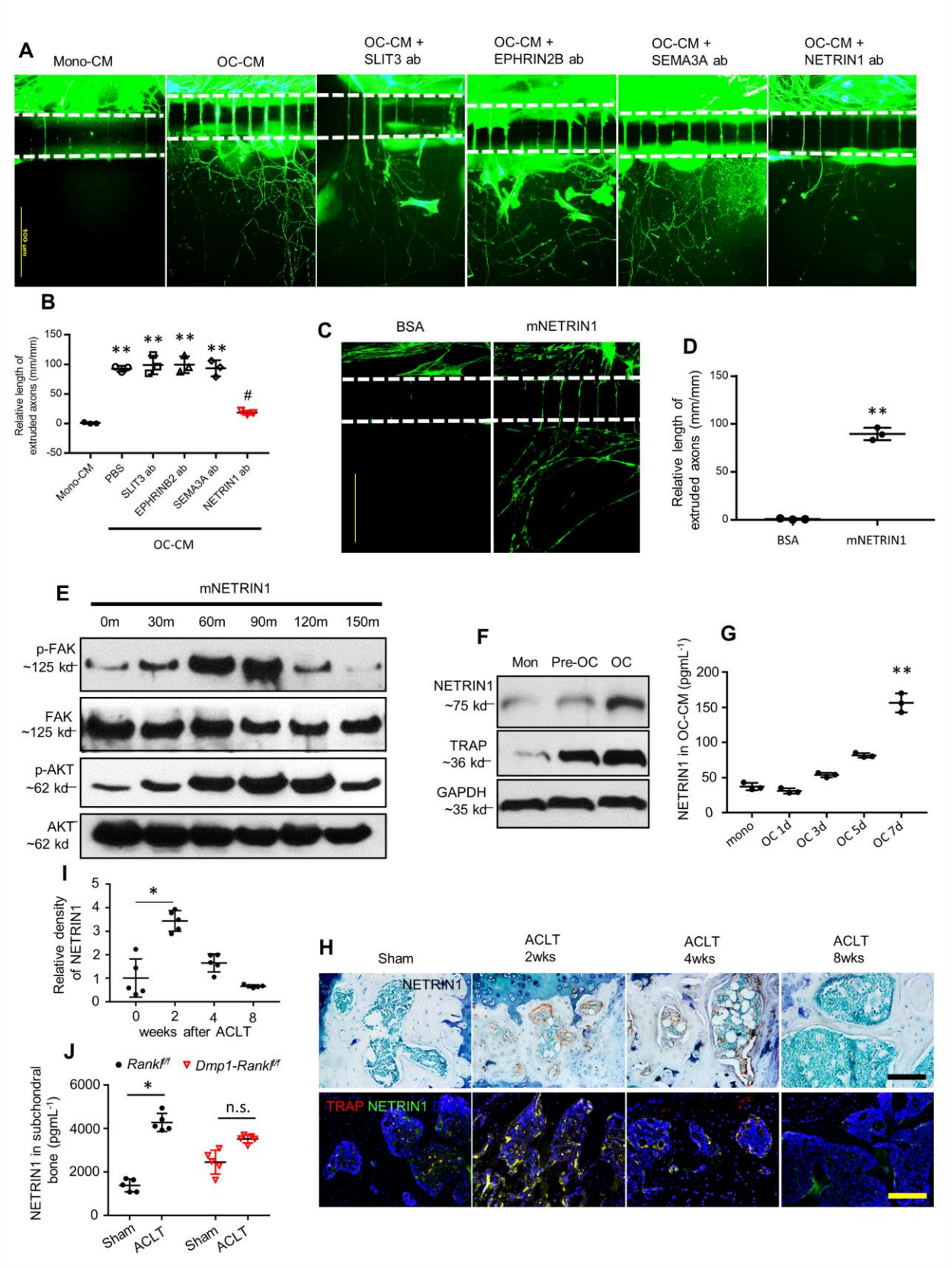
A
Mono-CM
OC-CM
OC-CM + SLIT3 ab
OC-CM + EPHRIN2B ab
OC-CM + SEMA3A ab
OC-CM + NETRIN1 ab
B
Relative length of extruded axons (mm/mm)
Mono-CM
PBS
SLIT3 ab
EPHRINB2 ab
SEMA3A ab
NETRIN1 ab
OC-CM
C
BSA
mNETRIN1
D
Relative length of extruded axons (mm/mm)
BSA
mNETRIN1
E
mNETRIN1
0m
30m
60m
90m
120m
150m
p-FAK ~125 kd
FAK ~125 kd
p-AKT ~62 kd
AKT ~62 kd
F
Mon
Pre-OC
OC
NETRIN1 ~75 kd
TRAP ~36 kd
GAPDH ~35 kd
G
NETRIN1 in OC-CM (pgmL-1)
mono
OC 1d
OC 3d
OC 5d
OC 7d
I
Relative density of NETRIN1
weeks after ACLT
J
Rankl f/f
Dmp1-Rankl f/f
NETRIN1 in subchondral bone (pgmL-1)
n.s.
Sham
ACLT
H
Sham
ACLT 2wks
ACLT 4wks
ACLT 8wks
NETRIN1
TRAP NETRIN1

Figure 4 NETRIN1 from osteoclasts induces axonal growth. **(A)** Microfluidics assay of osteoclast-conditioned medium promoting DRG neuron axonal growth with treatment of functional blocking antibodies. Mono-CM: monocyte-conditioned medium, OC-CM: osteoclast-conditioned medium, ab: antibody. Scale bar, 100 μm. **(B)** Quantification of the length of axons that protruded into axonal side. **p < 0.01 compared with mono-CM group, #p < 0.05 compared with OC-CM group**.** n = 3 per group. **(C)** Microfluidics assay of recombinant mouse NETRIN1 promoting DRG neuron axonal growth. Scale bar, 100 μm. **(D)** Quantification of the length of axons that protruded into axonal side. **p < 0.01 compared with BSA control group. n = 3 per group. **(E)** Western blots of the phosphorylation of FAK and AKT in DRG neurons treated with NETRIN1 for 0–150 min. **(F)** Western blots of NETRIN1 expression in monocytes, pre-osteoclasts and osteoclasts**. (G)** ELISA analysis of NETRIN1 concentration in conditioned media during osteoclast differentiation. **p < 0.01 compared with mono-CM group. **(H)** IHC staining of NETRIN1 and co-staining of NETRIN1 and TRAP in subchondral bone of WT mice at different time points after surgery. Scale bar, 100 μm. **(I)** Quantitative analysis of density of NETRIN1 in subchondral bone marrow. *p < 0.05 compared with the sham-operated group. **(J)** ELISA analysis of NETRIN1 concentration in subchondral bone marrow of *Rankl*$^{f/f}$ and *Dmp1-Rankl*$^{f/f}$ with or without ACLT surgery. *p < 0.05, n.s., no significant difference. Statistical significance was determined by multifactorial ANOVA, and all data are shown as means ± standard deviations.

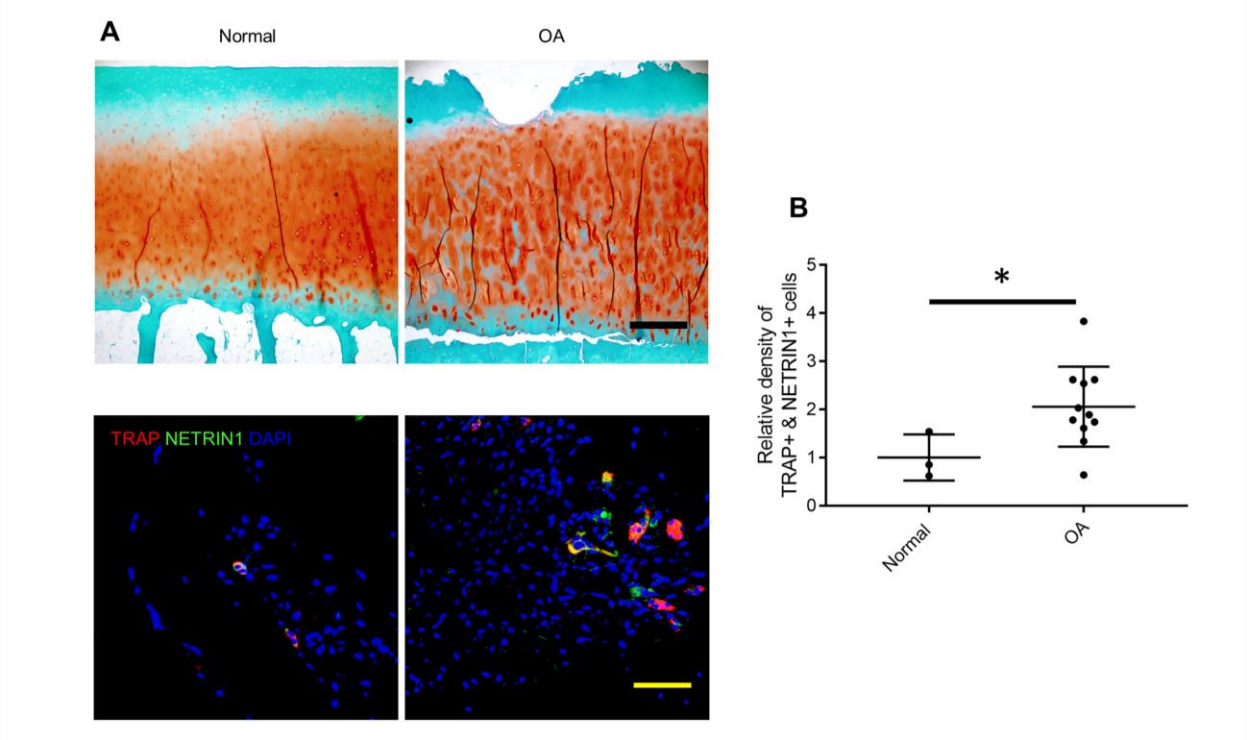

Figure 5 Osteoclast-derived NETRIN1 is elevated in human OA subchondral bone. **(A)** Top, safranin orange staining of human normal and OA cartilage and subchondral bone. Scale bar, 100 μm; Bottom, immunofluorescent staining of TRAP and NETRIN1 in human subchondral bone. Scale bar, 50 μm. **(B)** Quantitative analysis of relative intensity of TRAP and NETRIN1 double-positive cells in human subchondral bone. *$p < 0.05$ compared with healthy control.

	Normal	OA
Sample size	3	11
Gender	2M/1F	6M/5F
Height (cm)	172±3.4	169±2.9
Body weight (kg)	69±5.8	71±3.7
Age	33.2±4.5	56.8±2.7
BMI	22.4±2.7	23.8±1.6
Varus deformity (degree)	N/A	10.5±2.7
KL stage	0	2.9±0.7
KSS score	N/A	53.1±7.9

Table1 Information (including sample size, sex, height, body weight, age, BMI, varus deformity degree, KL stage, and KSS score) about the human samples.

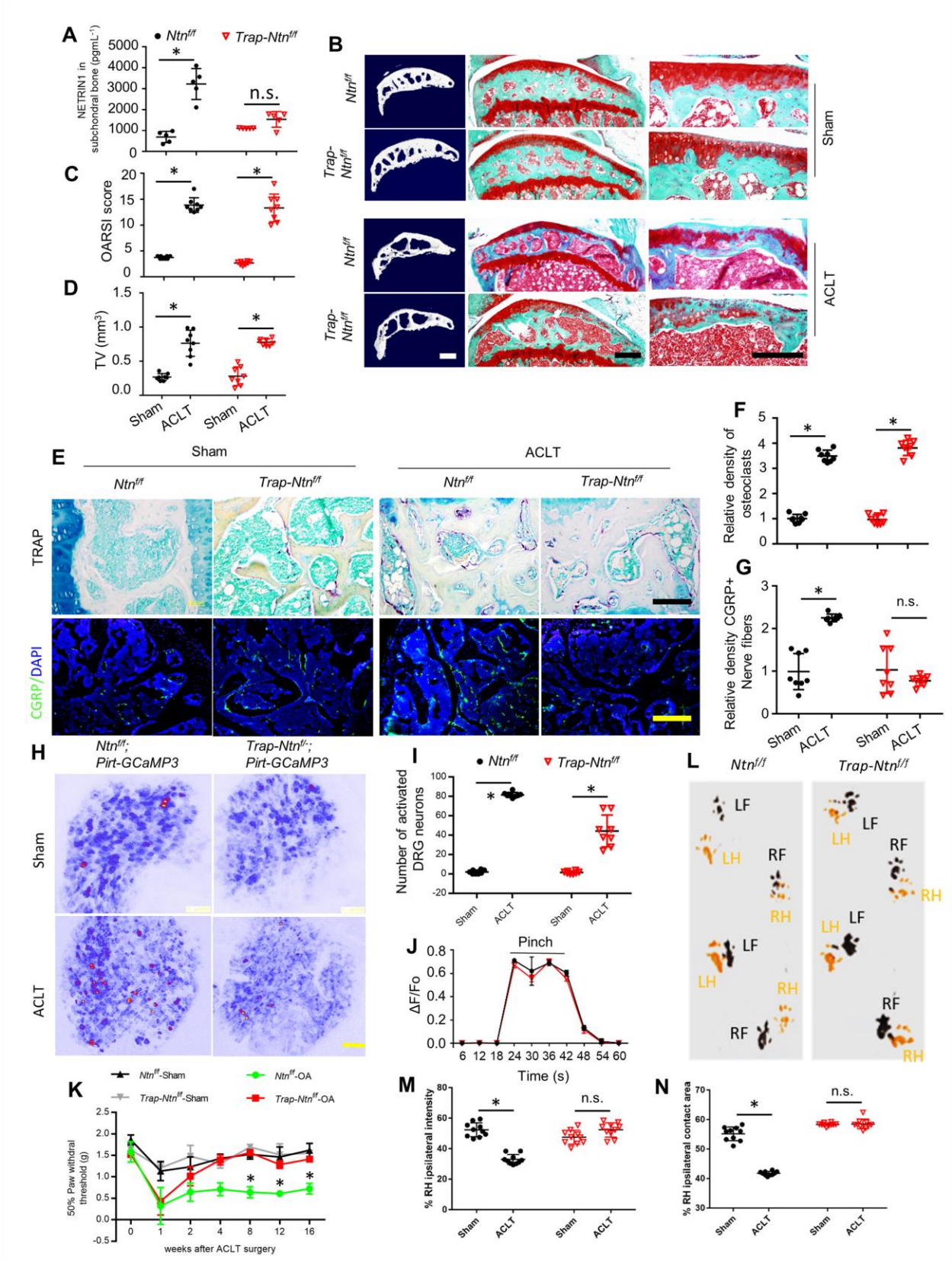
A
Ntn^f/f
Trap-Ntn^f/f
NETRIN1 in subchondral bone (pgmL-1)
5000
4000
3000
2000
1000
0
*
n.s.
B
Ntn^f/f
Trap-Ntn^f/f
Sham
ACLT
C
OARSI score
20
15
10
5
0
*
*
D
TV (mm3)
1.5
1.0
0.5
0.0
*
*
Sham
ACLT
Sham
ACLT
E
Sham
ACLT
Ntn^f/f
Trap-Ntn^f/f
Ntn^f/f
Trap-Ntn^f/f
TRAP
CGRP/DAPI
F
Relative density of osteoclasts
5
4
3
2
1
0
*
*
G
Relative density CGRP+ Nerve fibers
3
2
1
0
*
n.s.
Sham
ACLT
Sham
ACLT
H
Ntn^f/f; Pirt-GCaMP3
Trap-Ntn^f/-; Pirt-GCaMP3
Sham
ACLT
I
Ntn^f/f
Trap-Ntn^f/f
Number of activated DRG neurons
100
80
60
40
20
0
-20
*
*
Sham
ACLT
Sham
ACLT
J
Pinch
ΔF/Fo
0.8
0.6
0.4
0.2
0.0
6 12 18 24 30 36 42 48 54 60
Time (s)
K
Ntf/f-Sham
Trap-Ntnf/f-Sham
Ntf/f-OA
Trap-Ntnf/f-OA
50% Paw withdral threshold (g)
2.5
2.0
1.5
1.0
0.5
0.0
-0.5
*
*
*
0
1
2
4
8
12
16
weeks after ACLT surgery
L
Ntn^f/f
Trap-Ntn^f/f
LF
LH
RF
RH
M
% RH ipsilateral intensity
80
60
40
20
0
*
n.s.
Sham
ACLT
Sham
ACLT
N
% RH ipsilateral contact area
70
60
50
40
30
*
n.s.
Sham
ACLT
Sham
ACLT

Figure 6 Knockout of *Netrin1* in osteoclast lineage cells reduces sprouting of CGRP+ sensory nerves in subchondral bone and ameliorates OA pain. **(A)** ELISA analysis of NETRIN1 concentration in subchondral bone marrow of $Ntn^{f/f}$ and *Trap-*$Ntn^{f/f}$ with or without ACLT surgery. *p < 0.05, n.s., no significant difference. n = 5 per group. **(B)** Left, 3-dimensional μCT image of the tibial subchondral bone medial compartment (sagittal view) of $Ntn^{f/f}$ and *Trap-*$Ntn^{f/f}$ with or without ACLT surgery. Scale bar, 1 mm. Middle and right, safranin orange and fast green staining of articular cartilage in sagittal sections of tibia medial compartment of mice. Scale bars, 500 μm (middle) and 100 μm (right). **(C)** OARSI scores 8 weeks after surgery. *p < 0.05, *n* = 8 per group. **(D)** Quantitative analysis of total tissue volume (TV) in subchondral bone determined by μCT analysis. *n* = 8 per group. *p < 0.05, n.s. = no significant difference. **(E)** TRAP staining (top, magenta) and immunofluorescence analysis of CGRP+ sensory nerve fibers (bottom, green) in mouse tibial subchondral bone after ACLT surgery. Scale bar, 50 μm. **(F,G)** Quantitative analysis of relative density of TRAP+ osteoclast and CGRP+ nerve fibers in subchondral bone marrow. *p < 0.05. **(H)** *In vivo* calcium imaging in whole L4 DRG primary sensory neurons after mechanical press to knees of $Ntn^{f/f}$*;Pirt-GCaMP3* and *Trap-*$Ntn^{f/-}$*;Pirt-GCaMP3* ACLT mice. Scale bar, 50 μm. **(I)** Number of neurons activated by mechanical press. *p < 0.05. **(J)** Mean ± standard deviation of ΔF/Fo for neurons in a representative DRG responding to ~20-g knee pinch in $Ntn^{f/f}$ (black) and *Trap-*$Ntn^{f/-}$ (red) mice after ACLT. **(K)** Paw withdrawal threshold (PWT) was tested at the right hind paw of $Ntn^{f/f}$ and *Trap-*$Ntn^{f/f}$ mice with or without ACLT. *p < 0.05. **(L)** Representative copies of ink blotting trial of $Ntn^{f/f}$ and *Trap-*$Ntn^{f/f}$ mice after ACLT surgery on right knees. RH = right hind (orange), LH = left hind (orange), RF = right front (black), LF = left front (black). **(M,N)** Quantitative analysis of percentage RH ipsilateral intensity **(M)** and percentage RH ipsilateral contact area **(N)** by Image J software. *p < 0.05, n.s. = no significant

difference. n = 10 per group. Statistical significance was determined by multifactorial ANOVA, and all data are shown as means ± standard deviations.

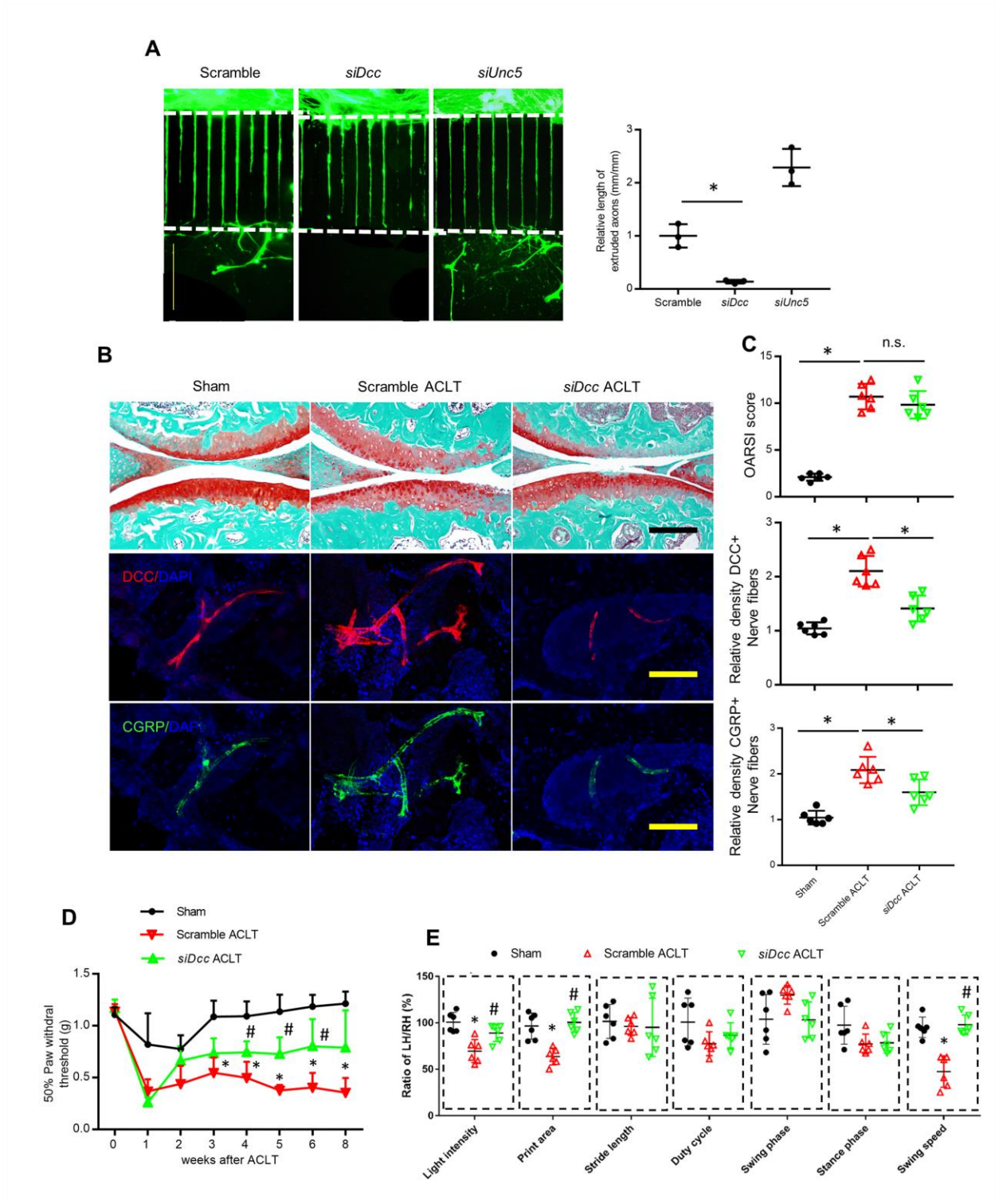

Figure 7 *In vivo* silencing of murine *Dcc* mRNA by siRNA systemic administration reduced CGRP+ sensory nerves subchondral bone innervation and OA pain. **(A)** Microfluidics assay of osteoclast-conditioned medium promoting DRG neuron axonal growth with treatment of *siDcc* and *siUnc5*. Scale bar, 100 μm. *p < 0.05. **(B)** Top, safranin orange and fast green staining of articular cartilage in sagittal sections of the tibia medial compartment of mice. Scale bar, 100 μm. Immunofluorescence analysis of DCC+ (middle, red) and CGRP+ (bottom, green) sensory nerve fibers in mouse tibial subchondral bone 4 weeks after surgery. Scale bars, 50 μm. **(C)** Quantitative analysis of OARSI score (top), relative density of DCC+ (middle) and CGRP+ (bottom) nerve fibers in subchondral bone marrow. *p < 0.05. n.s. = no significant difference. **(D)** Paw withdrawal threshold (PWT) was tested at the left hind paw of sham, scramble ACLT, and *siDcc* ACLT mice at different time points after surgery. *p < 0.05, compared with sham mice. #p < 0.05 compared with ACLT-operated and scramble siRNA-administered mice. **(E)** Variations in the ipsilateral and contralateral hind limbs of gait parameters obtained from CatWalk analysis. *p < 0.05, compared with sham mice. #p < 0.05 compared with ACLT-operated and scramble siRNA-administered mice. Statistical significance was determined by multifactorial ANOVA, and all data are shown as means ± standard deviations.

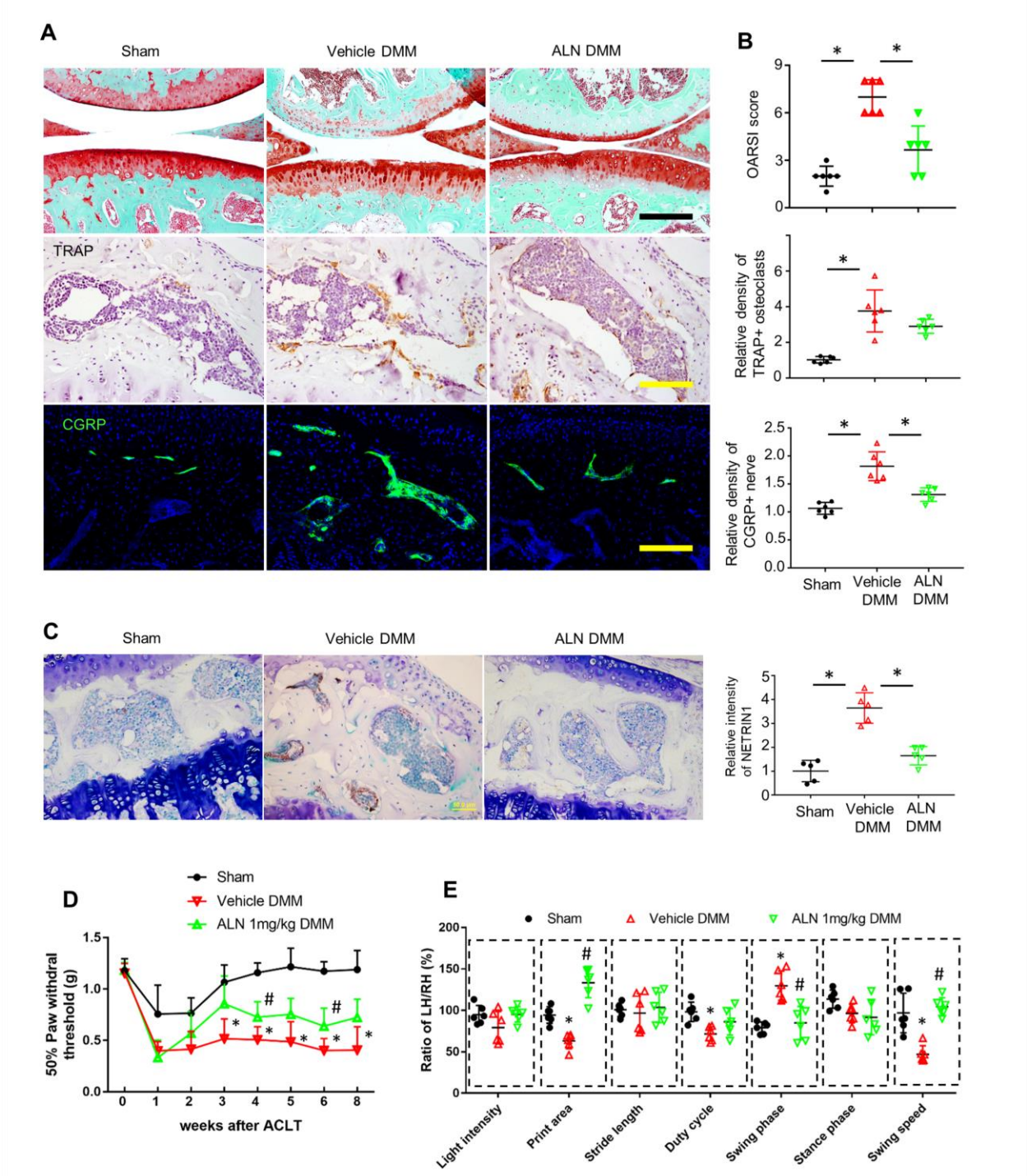

Figure 8 Effect of alendronate on DMM-induced OA pain. **(A)** Top, safranin orange and fast green staining of articular cartilage in sagittal sections of the tibia medial compartment of mice. Scale bar, 100 μm; middle and bottom, immunohistochemistry analysis of TRAP+ (middle) and immunofluorescence analysis of CGRP+ (bottom, green) sensory nerve fibers in mouse tibial

subchondral bone after DMM surgery. Scale bars, 50 μm. **(B)** Quantitative analysis of OARSI score (top), relative density of TRAP+ osteoclasts (middle) and CGRP+ (bottom) nerve fibers in subchondral bone marrow. *p < 0.05. **(C)** IHC staining and quantification of NETRIN1 in subchondral bone of Sham operated mice and DMM operated mice treated with either vehicle or ALN. Scale bar, 50 μm, *p < 0.05. **(D)** Paw withdrawal threshold (PWT) was tested at the left hind paw of sham, vehicle DMM, and ALN ACLT mice at different time points after surgery. *p < 0.05 compared with sham mice, #p < 0.05 compared with DMM-operated and vehicle-administered mice. **(E)** Variations in the ipsilateral and contralateral hind limbs of gait parameters obtained from CatWalk analysis. *p < 0.05, compared with sham mice. #p < 0.05 compared with DMM-operated and vehicle-administered mice. Statistical significance was determined by multifactorial ANOVA, and all data are shown as means ± standard deviations.